The Journal of Chemical Physics

The interaction-induced dipole of H_2–H: New *ab initio* results and spherical tensor analysis

Cite as: J. Chem. Phys. **150**, 204307 (2019); https://doi.org/10.1063/1.5098900
Submitted: 04 April 2019 . Accepted: 25 April 2019 . Published Online: 31 May 2019

Hua-Kuang Lee, Xiaoping Li, Evangelos Miliordos, and Katharine L. C. Hunt

The Journal of Chemical Physics ARTICLE scitation.org/journal/jcp

The interaction-induced dipole of H_2–H: New *ab initio* results and spherical tensor analysis

Cite as: J. Chem. Phys. 150, 204307 (2019); doi: 10.1063/1.5098900
Submitted: 4 April 2019 • Accepted: 25 April 2019 •
Published Online: 31 May 2019

Hua-Kuang Lee,[1] Xiaoping Li,[1] Evangelos Miliordos,[2] and Katharine L. C. Hunt[1,a)]

AFFILIATIONS

[1] Department of Chemistry, Michigan State University, East Lansing, Michigan 48824, USA
[2] Department of Chemistry and Biochemistry, Auburn University, Auburn, Alabama 36489, USA

[a)] huntk@msu.edu

ABSTRACT

We present numerical results for the dipole induced by interactions between a hydrogen molecule and a hydrogen atom, obtained from finite-field calculations in an aug-cc-pV5Z basis at the unrestricted coupled-cluster level including all single and double excitations in the exponential operator applied to a restricted Hartree–Fock reference state, with the triple excitations treated perturbatively, i.e., UCCSD(T) level. The Cartesian components of the dipole have been computed for nine different bond lengths r of H_2 ranging from 0.942 a.u. to 2.801 a.u., for 16 different separations R between the centers of mass of H_2 and H between 3.0 a.u. and 10.0 a.u., and for 19 angles θ between the H_2 bond vector **r** and the vector **R** from the H_2 center of mass to the nucleus of the H atom, ranging from 0° to 90° in intervals of 5°. We have expanded the interaction-induced dipole as a series in the spherical harmonics of the orientation angles of the H_2 bond axis and of the intermolecular vector, with coefficients $D_{\lambda L}(r, R)$. For the geometrical configurations that we have studied in this work, the most important coefficients $D_{\lambda L}(r, R)$ in the series expansion are $D_{01}(r, R)$, $D_{21}(r, R)$, $D_{23}(r, R)$, $D_{43}(r, R)$, and $D_{45}(r, R)$. We show that the *ab initio* results for $D_{23}(r, R)$ and $D_{45}(r, R)$ converge to the classical induction forms at large R. The convergence of $D_{45}(r, R)$ to the hexadecapolar induction form is demonstrated for the first time. Close agreement between the long-range *ab initio* values of $D_{01}(r_0 = 1.449$ a.u., R) and the known analytical values due to van der Waals dispersion and back induction is also demonstrated for the first time. At shorter range, $D_{01}(r, R)$ characterizes isotropic overlap and exchange effects, as well as dispersion. The coefficients $D_{21}(r, R)$ and $D_{43}(r, R)$ represent anisotropic overlap effects. Our results for the $D_{\lambda L}(r, R)$ coefficients are useful for calculations of the line shapes for collision-induced absorption and collision-induced emission in the infrared and far-infrared by gas mixtures containing both H_2 molecules and H atoms.

I. INTRODUCTION

When a hydrogen molecule and a hydrogen atom collide, their interactions distort the charge distributions of both H_2 and H, producing a transient dipole during the collision.[1–5] We have investigated the dependence of the interaction-induced dipole of the H_2–H system on the bond length r of H_2, the separation R between the centers of mass of H_2 and H, and the angle θ between the H_2 bond axis **r** and the vector **R** connecting the center of mass of H_2 to the nucleus of the H atom.

The interaction energy of a hydrogen molecule with a hydrogen atom has been evaluated in multiple *ab initio* calculations of high accuracy,[6–15] with nonadiabatic corrections included;[16–18] however, we have found only two previous *ab initio* calculations of the dipole moment of H_2–H. In 1973, Patch obtained the H_2–H dipole at a full configuration-interaction (CI) level but in a minimal basis of three 1s functions.[19] Patch determined the dipole for six relative orientations of H_2–H and four separations between the H atom and the H_2 center of mass, ranging from 1.0 a.u. to 4.0. a.u.[19] All of these calculations were carried out with an H_2 bond length r of 1.401 446 a.u.[19] In 2003, Gustafsson, Frommhold, and Meyer (GFM) carried out a substantially more extensive study using a larger basis, variable bond lengths, and a wider range of H_2 to H separations.[20]

Our work is larger in scale than either previous study. We have calculated the interaction-induced dipole for 19 different angles θ from 0° to 90° in intervals of 5° vs four angles (0°, 30°, 60°, and 90°) used by GFM.[20] Symmetry arguments make it possible to determine the dipole over the full range of angles out to 360°, based on the results from 0° to 90°. Our calculations cover nine different bond

lengths of H_2 from 0.942 a.u. to 2.801 a.u., while the GFM study covered five bond lengths from 1.111 a.u. to 1.787 a.u.[20] We have also carried out calculations for a total of 16 different separations between H_2 and H, from 3.0 a.u. to 10.0 a.u. vs 11 separations in the GFM work. Our calculations cover a total of 2736 geometrical configurations of H_2–H. We have determined the dipole by finite-field methods with Molpro;[21] the dipoles reported in the current work have been obtained from more than 43 000 *ab initio* calculations all together.

We have converted the interaction-induced Cartesian dipoles to a spherical-tensor form. Then, we have fit the results to a series in the spherical harmonics $Y_\lambda^\mu(\Omega_r)$ of the orientation angles Ω_r of the H_2 bond axis **r** and the spherical harmonics $Y_L^m(\Omega_R)$ of the orientation angles of the intermolecular vector **R**.[22–25] The coefficients $D_{\lambda L}(r, R)$ in this series depend only on λ, L, and the magnitudes of the bond length r and the H_2–H separation R. The contributions to the dipole from various polarization mechanisms are separated out in the coefficients $D_{\lambda L}(r, R)$.[22–25] From the angle dependence of the interaction-induced dipole, we have determined the $D_{\lambda L}$ coefficients D_{01}, D_{21}, D_{23}, D_{43}, D_{45}, D_{65}, D_{67}, D_{87}, and D_{89}. The coefficient $D_{01}(r, R)$ gives the contribution to the H_2–H dipole that is isotropic in the orientation of the H_2 molecule. At long range, $D_{01}(r, R)$ gives the dominant term in the van der Waals dispersion dipole.[26–34] At short range, $D_{01}(r, R)$ characterizes exchange and overlap effects, as well as dispersion. At long range, the coefficient $D_{23}(r, R)$ is determined by quadrupolar induction,[22–25] while at short range, $D_{23}(r, R)$ is affected by anisotropic induction, overlap damping, and exchange effects. The coefficient $D_{45}(r, R)$ plays the analogous role for hexadecapolar induction.[23–25] The leading long-range terms in the coefficients $D_{21}(r, R)$ and $D_{43}(r, R)$ vary as R^{-7} in the H_2–H separation,[23] but at short range, the relative importance of $D_{21}(r, R)$ and $D_{43}(r, R)$ increases, especially for the larger bond lengths r. These coefficients reflect anisotropic overlap and exchange effects on the total dipole moment.

The spherical harmonic series is needed to determine the line shapes for absorption and emission in the infrared and far infrared, due to the transient dipole that exists during collisions of H_2 molecules with H atoms.[1–5,19,20,35,36] Collision-induced absorption,[1–5,37–74] emission,[75–79] light scattering,[80–92] and nonlinear Rayleigh and Raman scattering processes[93] have been investigated experimentally for H_2 interacting with helium atoms,[41–48] with other inert gas atoms,[44,45,49–54] with H_2 molecules,[46–48,55–74] or with other species, including CO,[94–98] CO_2,[99] CH_4,[100–104] N_2,[96,104–106] NH_3,[107] and O_2.[54] The interaction effects on collision-induced spectra involving the isotopic variants HD and D_2 have been studied experimentally,[108–125] as well as interaction effects on the spectra of bound H_2 dimers[126–130] and of bound complexes of H_2 with other molecules.[131–138] Simultaneous vibrational transitions in all three molecules of an H_2–H_2–H_2 cluster have been observed experimentally;[140] these must be a consequence of irreducible three-body interactions.[141–144] Interaction-induced transitions have also been studied in solid hydrogen,[145–154] which shows rotational state changes with $\Delta J = 4$ (Ref. 153) and $\Delta J = 6$ (Ref. 154).

Rich and McKellar[155] compiled an early bibliography of research on collision-induced absorption, starting with the first observation of the phenomenon in O_2 gas by Crawford, Welsh, and Locke,[37] followed shortly by the first observation of the rotovibrational infrared spectrum of H_2,[38] and continuing with the first detections of the collision-induced vibrational overtone in H_2 gas[39] and of the pure rotational absorption spectrum of H_2.[40] The bibliography was updated by Hunt and Poll in 1986.[156] An overview of recent work in the field was provided by Hartmann and coworkers in 2018.[5] Borysow and Frommhold compiled a bibliography of work on collision-induced light scattering through 1989.[157] The literature on collision-induced absorption or emission, collision-induced light scattering, and collision-induced hyper-Rayleigh scattering or hyper-Raman scattering is quite extensive, even if limited to spectroscopic processes involving H_2 or one of its isotopic variants.

The interaction-induced dipoles,[158–170] interaction-induced polarizabilities,[166–168,170–174] and interaction-induced hyperpolarizabilities[166,167,170,171,175–177] that give rise to the collision-induced spectra for these species have been calculated with high accuracy *ab initio*, starting with work by Meyer, Frommhold, Borysow, and Birnbaum.[158–165] For collision-induced absorption by H_2–He and H_2–H_2, excellent agreement has been attained between experimental spectra and spectra calculated from *ab initio* results for the interaction-induced dipoles (see Refs. 158–160, 162–165, 168, and 178–182). A high level of agreement has also been found between the experimental and calculated collision-induced spectra of other molecules,[183,184] including collision-induced vibronic transitions in O_2–O_2 and O_2–N_2.[185,186] In addition, spectra have been successfully calculated with intermolecular potentials derived from transport coefficients.[187–190]

Theory and experiment have converged in determining the scattering cross sections of H_2 molecules and H atoms, based on calculations of the potential energy surface and quantum scattering theory,[191] but theoretical work remains the sole source of information on the H_2–H *dipole* to date. The H_2–H complex is of interest as the smallest open-shell system where classical induction contributes to the dipole, in addition to exchange, overlap, and van der Waals dispersion effects. Comparisons of the H_2–H dipole with the dipole of the small closed-shell system H_2–He[169] are included in this work.

Information on the energy of H_2 interacting with an H atom is used to model processes in galactic gas clouds, stars, and planets with atmospheres that contain both hydrogen molecules and hydrogen atoms.[192] Collision-induced absorption by H_2–H_2 and H_2–He pairs[193–196] and the absorption spectra of dimers[197–199] are known to have astrophysical significance. For example, very old, very cool white dwarf stars emit less radiation in the infrared than predicted, based on the Planck radiation law and the temperatures of the stellar cores.[194–196] The reduced intensity of emitted IR radiation is attributed to collision-induced absorption by H_2–H_2 and H_2–He in the stellar atmospheres.[194–196,200–205] Results for the H_2–H_2 and H_2–He spectra have been included in the HITRAN database maintained by the Harvard-Smithsonian Center for Astrophysics.[206] Effects of the interactions between H_2 molecules and H atoms have been detected in the spectra of DA white dwarf stars,[207,208] with outer shells of pure hydrogen. For these stars, a previously unexplained intensity of radiation in the ultraviolet has been traced to pressure-broadening of the Lyman alpha bands of H atoms, due to collisions with H_2.[207,208] The H_2–H interactions alter both the transition dipole and the transition energy between the ground and excited states

of the H atom. The current work focuses on a different property, the collision-induced dipole of H_2–H in the ground electronic state. Collision-induced absorption by H_2–H would occur in the same spectral region as absorption by H_2–H_2 or H_2–He.

While the transition from atomic to molecular hydrogen is rather sharp under equilibrium conditions of astrophysical relevance,[209] under nonequilibrium conditions, H_2 and H may be present together in appreciable quantities.[210–212] For example, star formation is driven by processes involving molecular hydrogen in cool galactic gas clouds;[213] yet recent observations suggest that "atomic hydrogen has been dominating the cold-gas mass budget of star forming galaxies for at least the past three billion years."[214] Large gas reservoirs of atomic hydrogen have been detected in galaxies at red-shifts between 0.01 and 0.05 (Ref. 215) and between 0.17 and 0.25 (Ref. 216). Atomic hydrogen fractions are correlated with galactic dynamics, including recent mergers[217] and disk-specific values of the angular momentum.[218]

Molecular and atomic hydrogen are both found in the atmospheres of Jupiter,[219] Saturn, and Saturn's rings.[220] Atomic hydrogen coronas have been detected around Ganymede,[221,222] Callisto,[223] Europa,[224] Io,[225] and Titan.[226] Atomic hydrogen has also been detected at distances of ~250 km from the surface of the Earth, closer than previously anticipated.[227] Extrasolar "hot Jupiters" such as HD 209458b,[228–231] HD 17156b,[232] and HD 189733b[233] show high concentrations of H atoms along with H_2; for example, the concentration of H atoms in the atmosphere of HD 209458b is reported to be three orders of magnitude higher than in Jupiter's atmosphere.[228–231] The loss of H atoms from these exoplanets into space is a primary atmospheric escape mechanism[234,235] leading to mass loss by the planets. "Warm Neptunes"[236,237] have also been observed; GJ 436b exhibits a "giant comet-like cloud of hydrogen" escaping from the planet, and GJ 3470b shows detectable Rayleigh scattering that suggests a hydrogen/helium composition of the atmosphere. Collectively, these observations suggest that our results for the interaction-induced dipole of H_2–H may find applications in astrophysical models.

In Sec. II of this paper, we describe our computational method and provide results for the Cartesian components of the dipole moment. Full results for the set of geometrical configurations in this work are included in the supplementary material deposited online. In Sec. III, we provide and analyze the results for the spherical-tensor coefficients $D_{\lambda L}(r, R)$, again with full results in the supplementary material. Also in Sec. III, we check for convergence of D_{23}, D_{45}, and D_{01} to their known long-range forms. In both Secs. II and III, we compare our results with the earlier GFM calculations of the H_2–H dipole. Section IV contains a brief summary, comparisons with the collision-induced dipole of H_2–He, and conclusions.

II. COMPUTATIONAL METHOD AND RESULTS FOR CARTESIAN COMPONENTS OF THE H_2–H DIPOLE

We used an aug-cc-pV5Z basis[238,239] and Molpro 2006[21] for our first set of production runs. We generated a wave function for the ground doublet state at the restricted Hartree–Fock (RHF) level and then constructed the unrestricted coupled-cluster wave function from that reference function[240] by including all single and double excitations in the exponential operator applied to the reference wave function, plus triple excitations treated perturbatively, defining the RHF/UCCSD(T) level.[241–243] From the RHF/UCCSD(T) energies, we obtained the dipole by finite-field methods, as opposed to direct calculation of the expectation value of the dipole moment.

For open-shell systems, spin-unrestricted calculations typically yield more accurate energies than restricted calculations (where the orbitals for α and β spins are identical), especially when bonds are stretched or broken, but the wave functions in the spin-unrestricted case are not eigenfunctions of $\mathbf{S}^2$. They may be contaminated by other spin states (see Ref. 244). Spin contamination of the doublet state by the quartet does not pose a problem in our calculations of the collision-induced dipole. Energies obtained from RHF/UCCSD(T) calculations with a spin-unprojected wave function are identical to the energies obtained from a spin-projected wave function, as shown by Rittby and Bartlett[245] and by Scuseria.[246] The wave functions are spin-contaminated, but the energies are correct for the spin state of interest. Therefore, our finite-field results for the dipole should be unaffected by spin-contamination. Schlegel[247] had shown that in a coupled-cluster calculation that starts from an unrestricted Hartree–Fock (UHF) reference state, the contamination of the wave function for one spin value by the next higher spin value S does not affect the energies. Since the H_2–H system has a doublet ground state, and no spin states of H_2–H with $S > 3/2$ are possible, a spin-unrestricted UHF reference state could have been used in the calculations, without causing spin contamination. In practice, we used the RHF/UCCSD(T) method implemented in Molpro.[21] The Molpro code uses the perturbative triples defined by Watts, Gauss, and Bartlett[242] although triples corrections of the type defined by Deegan and Knowles[243] are also generated automatically.

Our first calculations were carried out with the default convergence criteria: 10^{-6} for the energy, 10^{-12} for the two-electron integrals, 10^{-12} for numerical zero, 10^{-12} for neglect of small two-electron integrals, and 10^{-4} for the coefficients in the UCCSD(T) wave function.[248] The calculations were run for H_2 to H separations of 3.4–4.0 a.u. in steps of 0.1 a.u., at 4.2 a.u. and 4.5 a.u., and then for 5.0 a.u.–10.0 a.u. in steps of 1.0 a.u. We set the bond lengths for the H_2 molecule to 0.942, 1.111, 1.280, 1.449, 1.787, 2.125, 2.463, or 2.801 a.u. to facilitate the comparison with earlier calculations.[20] The averaged bond length in the ground rovibrational state of H_2 is 1.449 a.u.

We calculated the energies for six different values of a uniform field applied in the z direction (along **R**) and in the direction orthogonal to **z** in the plane containing H_2–H. The field strengths were obtained from a reference electric-field value f by taking f, −f, $2^{1/2}$ f, $-2^{1/2}$ f, $3^{1/2}$ f, and $-3^{1/2}$ f.[249] In the initial study, we set f = 0.002 a.u. The combinations ±f, $\pm 2^{1/2}$ f, and $\pm 3^{1/2}$ f make it possible to eliminate terms of even order in f from the calculated dipole. With results for six field strengths, we removed the odd-order hyperpolarization terms of orders f^3 and f^5, so the leading-order hyperpolarization effect that remains is O (f^7). The RHF/UCCSD(T) results were obtained first for zero field and then for each of the fields listed above in sequence, using the converged orbitals from the previous calculation as the starting point for the next. Generally, this approach works quite well, but this sequence of calculations does not ensure precise equality between the energies calculated in fields f and −f perpendicular to **R**, for the linear and T-shaped configurations. In the first set of calculations, we obtained small, but

nonzero dipole components perpendicular to **R** for T-shaped configurations when the bond length and the H_2–H separations were both large.

We therefore undertook a second set of calculations with the aug-cc-pV5Z basis,[238,239] using Molpro 2012 and tighter convergence criteria: 10^{-12} for the energy, 10^{-12} for the two-electron integrals (the default value), 10^{-14} for numerical zero, 10^{-5} for the coefficients in the UCCSD(T) wave function, and 10^{-10} for the density matrix. Results of these calculations are denoted by A5Z†. With the tighter convergence thresholds, the symmetry requirements were met to at least six decimal places in the calculated dipoles. These calculations were run for nine H_2 bond lengths (adding r = 1.618 a.u. to our previous set), eight H_2–H separations R (from 3.0 to 10.0 a.u. in steps of 1.0 a.u.), and 19 angles θ. The base field strength f for these calculations was 0.002 a.u., as above. As a check on the results, calculations were run at r = 1.449 a.u. with the larger basis sets aug-cc-pV6Z and d-aug-cc-pV5Z.[238,239] As an additional check, calculations were run for two geometrical configurations using Molpro 2015, the aug-cc-pV6Z basis, the tighter convergence criteria, and base field strengths f of 0.001 a.u. and 0.01 a.u.

The aug-cc-pV5Z basis has 8s, 4p, 3d, 2f, and 1g functions contracted to 5s, 4p, 3d, 2f, and 1g functions on each H center, for a total of 165 contracted functions for the H_2–H system. In addition to accounting for the interaction-induced polarization along the vector **R** from the center of mass of H_2 to the nucleus of the H atom, this basis should be flexible in representing the polarization perpendicular to **R**, which is nonzero when θ is different from 0° or 90°.

Our full results from the first and second sets of calculations are listed in Tables S1–S9 in the supplementary material. Results from calculations with the tighter convergence criteria are indicated by a superscript †. Tables S1–S9 are organized in order by bond length, from Table S1 for r = 0.942 a.u. through Table S9 for r = 2.801 a.u. The results in each table are grouped by angle; then, for each angle, results are listed for a total of 16 separations R between the centers of mass of H_2 and H. The vector from the center of mass of H_2 to the nucleus of the H atom points vertically up along z. For the calculations in these tables, the H_2–H complex lies in the yz plane, and the positive y axis points to the right, as shown in Fig. 1.

When the distance r between the nuclei in H_2 is greater than or equal to 2.125 a.u. and R and θ are both small, the correct nuclear coordinates are still given by the nominal label H_2–H, but the system should be identified as H_3, H–H_2 (pairing different H nuclei into H_2), or H–H–H. The dipoles μ_y and μ_z are tabulated in these cases, but to indicate that they do not refer to H_2–H, the results are printed in red in Tables S1–S9. In a small number of cases, no value is listed because the calculations did not converge.

To exemplify the results, values obtained from the first and second sets of calculations for a bond length r of 1.449 a.u. (the average bond length in the ground rovibrational state) are listed in Table I for R from 4.0 a.u. to 10.0 a.u. and for angles θ from 0° to 90° in steps of 15°. This table contains 84 nonzero values of μ_y and μ_z from the two main sets of calculations. The corresponding results agree to 10^{-6} a.u. in 51 of the 84 cases, differ by $\pm 1 \times 10^{-6}$ a.u. in 18 additional cases, and differ by more than $\pm 1 \times 10^{-6}$ a.u. but agree to 10^{-5} a.u. in the remaining 15 cases. In two cases of the last set, the difference between the two calculations is just $\pm 2 \times 10^{-6}$ a.u. The largest differences are found for the dipole when R = 9.0 a.u. or 10.0 a.u., where the results from the calculations with the tighter convergence criteria (identified by the superscript † in the column headers) are preferable.

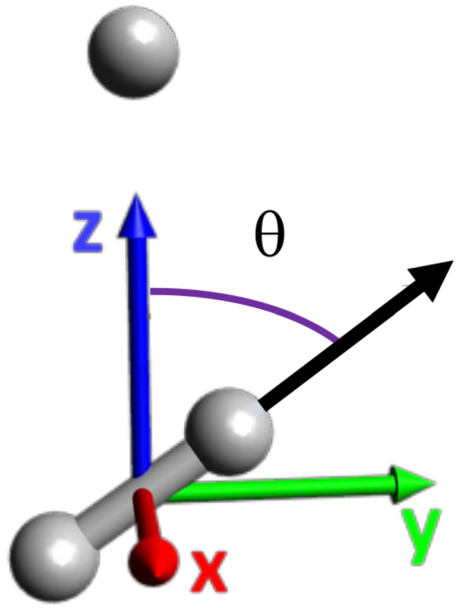

FIG. 1. Geometrical configuration of the H_2–H complex in the yz plane. The H_2 bond length is r, the separation between the centers of mass of H_2 and H is R, and the angle between the z axis along **R** and the H_2 bond axis is θ.

Significant features of the results for the Cartesian components of the collision-induced dipole are described next. Details on the dependence of the dipole components on r, R, and θ are presented in the supplementary material. The y component of the dipole is negative for all angles θ from 5° to 85°, when 3.0 a.u. ≤ R ≤ 10.0 a.u. and r ≤ 1.787 a.u., but in some cases, μ_y is positive at short range for larger bond lengths. The absolute value $|\mu_y|$ of the dipole in the y direction tends to decrease with increasing H_2–H separation R at constant r and θ; this is true for all r ≤ 1.618 a.u. and any angle θ. From θ = 0° to θ = 90° at constant R and r, the absolute value of μ_y increases monotonically with increasing θ to a maximum between θ = 30° and θ = 45° and then decreases monotonically with further increases in θ. Figure 2 shows $|\mu_y|$ as a function of θ and R when r = 2.125 a.u. For R ≥ 6.0 a.u., the absolute value of μ_y increases monotonically with bond length r over the full range from 0.942 a.u. to 2.801 a.u. at constant θ.

The dipole component μ_y shows the expected behavior for a quadrupole-induced dipole at long range. Exceptions with positive values of μ_y have been found at short range, for large bond lengths r and moderate to large angles θ. The exceptions at short range are consistent with substantial *positive* contributions to μ_y from exchange and overlap. These contributions become increasingly important as r increases and as the H_2 molecule rotates toward the y axis (while 0° < θ < 90°), causing the H nucleus in H_2 that has a positive z coordinate to move further out in the +y direction.

TABLE I. Cartesian dipole components of H_2–H for H_2 bond length r = 1.449 a.u.; R denotes the separation between the centers of mass of H_2 and H along the z axis, and θ is the angle between the H_2 bond axis **r** and the z axis pointing along **R**. Results labeled † have been obtained with an aug-cc-pV5Z basis set using Molpro 2012 and convergence criteria tighter than the default criteria (see text).

R	μ_y †	μ_y	μ_z †	μ_z
θ = 0°				
4.0	0	0	−0.011 906	−0.011 907
5.0	0	0	0.002 905	0.002 904
6.0	0	0	0.003 829	0.003 829
7.0	0	0	0.002 683	0.002 683
8.0	0	0	0.001 689	0.001 690
9.0	0	0	0.001 064	0.001 069
10.0	0	0	0.000 693	0.000 696
θ = 15°				
4.0	−0.004 294	−0.004 294	−0.014 923	−0.014 923
5.0	−0.002 243	−0.002 243	0.001 540	0.001 539
6.0	−0.001 234	−0.001 234	0.003 205	0.003 205
7.0	−0.000 702	−0.000 702	0.002 368	0.002 369
8.0	−0.000 416	−0.000 416	0.001 513	0.001 515
9.0	−0.000 260	−0.000 260	0.000 957	0.000 963
10.0	−0.000 170	−0.000 171	0.000 625	0.000 614
θ = 30°				
4.0	−0.007 211	−0.007 211	−0.022 959	−0.022 960
5.0	−0.003 811	−0.003 811	−0.002 064	−0.002 065
6.0	−0.002 101	−0.002 101	0.001 544	0.001 544
7.0	−0.001 194	−0.001 194	0.001 524	0.001 524
8.0	−0.000 708	−0.000 708	0.001 038	0.001 038
9.0	−0.000 442	−0.000 442	0.000 669	0.000 662
10.0	−0.000 290	−0.000 291	0.000 438	0.000 428
θ = 45°				
4.0	−0.008 003	−0.008 003	−0.033 411	−0.033 412
5.0	−0.004 298	−0.004 298	−0.006 694	−0.006 694
6.0	−0.002 381	−0.002 381	−0.000 614	−0.000 614
7.0	−0.001 355	−0.001 355	0.000 409	0.000 409
8.0	−0.000 805	−0.000 805	0.000 404	0.000 404
9.0	−0.000 503	−0.000 503	0.000 280	0.000 273
10.0	−0.000 330	−0.000 331	0.000 186	0.000 176
θ = 60°				
4.0	−0.006 677	−0.006 677	−0.043 229	−0.043 229
5.0	−0.003 638	−0.003 638	−0.011 002	−0.011 002
6.0	−0.002 025	−0.002 025	−0.002 654	−0.002 654
7.0	−0.001 156	−0.001 156	−0.000 662	−0.000 662
8.0	−0.000 689	−0.000 688	−0.000 210	−0.000 210
9.0	−0.000 430	−0.000 430	−0.000 101	−0.000 108
10.0	−0.000 282	−0.000 283	−0.000 063	−0.000 072

TABLE I. (*Continued.*)

R	μ_y †	μ_y	μ_z †	μ_z
θ = 75°				
4.0	−0.003 755	−0.003 754	−0.050 009	−0.050 007
5.0	−0.002 065	−0.002 065	−0.013 964	−0.013 964
6.0	−0.001 154	−0.001 153	−0.004 075	−0.004 075
7.0	−0.000 661	−0.000 661	−0.001 419	−0.001 419
8.0	−0.000 394	−0.000 394	−0.000 647	−0.000 647
9.0	−0.000 247	−0.000 247	−0.000 374	−0.000 381
10.0	−0.000 162	−0.000 163	−0.000 243	−0.000 252
θ = 90°				
4.0	0	0	−0.052 405	−0.052 404
5.0	0	0	−0.015 011	−0.015 010
6.0	0	0	−0.004 580	−0.004 580
7.0	0	0	−0.001 690	−0.001 690
8.0	0	0	−0.000 805	−0.000 805
9.0	0	0	−0.000 473	−0.000 480
10.0	0	0	−0.000 308	−0.000 317

The dipole component in the z direction (along **R**) typically changes sign from negative to positive as R increases, for θ < 50° and r ≤ 2.125 a.u. Exceptions are found for several of the values of μ_z listed in red in Tables S1–S9. Figure 3 shows μ_z as a function of θ and R, at r = 1.449 a.u. When θ ≥ 60°, $|\mu_z|$ decreases monotonically with increasing R, for r from 0.942 to 2.125 a.u. When θ ≤ 55°, $|\mu_z|$ typically decreases with increasing R, then increases, and finally decreases again, a pattern that holds in a little over 90% of the cases. The sign changes in μ_z in this case lead to a complex pattern of variations with r at fixed R and θ.

If μ_z were determined by quadrupolar induction effects alone, then we would find $\mu_z > 0$ when $\theta < \theta_m$, and $\mu_z < 0$ when $\theta > \theta_m$. Here, θ_m denotes the quadrupole "magic angle," where the quadrupole field in the z direction vanishes [$3\cos^2(\theta_m) - 1 = 0$, $\theta_m \approx 54.7356°$]. This pattern of signs is generally followed at long range. For

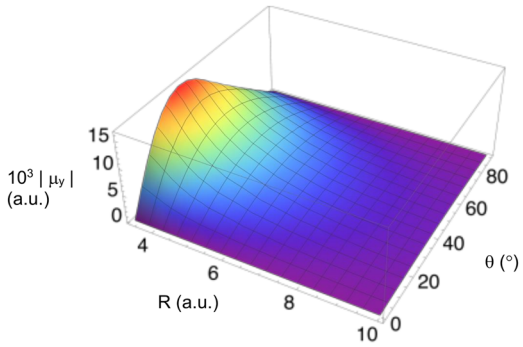

FIG. 2. Absolute value of μ_y for H_2–H multiplied by 10^3 (in a.u.), for R between 3.4 a.u. and 10.0 a.u. and θ between 0° and 90°, at bond length r = 2.125 a.u.

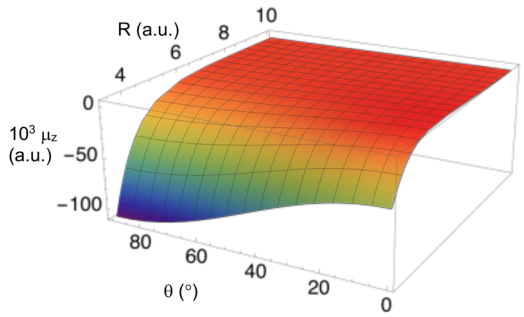

FIG. 3. Dipole component μ_z for H_2–H multiplied by 10^3 (in a.u.) for R from 3.4 to 10.0 a.u. and θ decreasing from 90° to 0°, at r = 1.449 a.u. Each point on this surface has a potential energy ΔE above the minimum for H_2–H that satisfies $\Delta E \leq k_B T$ at T = 2600 K.

example, Fig. 4 shows μ_y and μ_z as functions of θ at R = 10.0 a.u. and r = 1.449 a.u. The results from θ = 0° to θ = 90° have been calculated directly *ab initio*, and results for larger θ have been deduced by symmetry. The oscillatory pattern characteristic of quadrupolar induction is evident in this figure.

At short range (small R), the observed sign pattern of μ_z is somewhat different, for $\theta < \theta_m$ and r from 0.942 to 1.787 a.u. We find $\mu_z < 0$ in cases where the quadrupolar induction model would predict positive values of μ_z. In this range, there must be *negative* overlap and exchange contributions to μ_z that exceed the damped quadrupolar induction effects. But as R increases, μ_z converts to positive values for $\theta < \theta_m$, consistent with quadrupolar induction. The value of R where μ_z first becomes positive ranges from 3.9 a.u. to 9.0 a.u. for the bond lengths listed above.

For $\theta > \theta_m$, the quadrupole induction mechanism gives $\mu_z < 0$. From the calculations, we have found $\mu_z < 0$ for all $\theta \geq 60°$ when the bond length r is between 0.942 and 1.787 a.u. inclusive, and $\mu_z < 0$ for all $\theta \geq 55°$ when r = 2.125, 2.463, or 2.801 a.u. (except when R = 3.0 a.u. and r = 2.801 a.u.). The overlap and exchange contributions to μ_z when $\theta \geq 60°$ cannot be deduced on the basis of sign arguments alone, but the opposite signs of the short-range exchange and overlap effects for μ_y and μ_z in cases with $\theta < \theta_m$ suggest that the H atom gains a partial negative charge at short range, while the

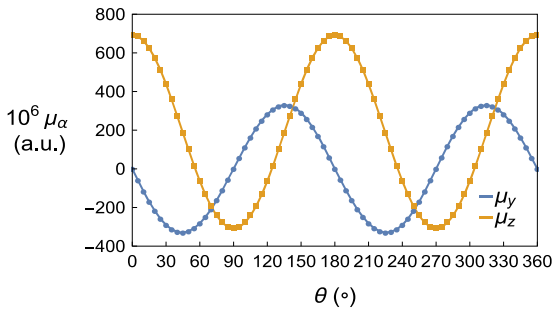

FIG. 4. Dipole components μ_y and μ_z for H_2–H vs θ for R = 10.0 a.u. and r = 1.449 a.u.

TABLE II. Comparison of Cartesian components of the dipole moment of H_2–H in this work with the results of Gustafsson, Frommhold, and Meyer (GFM).[20] We have reoriented the H_2–H complex in our work to correspond to the orientation used by GFM. Results are listed from our calculations with the aug-cc-pV5Z basis set, Molpro 2012, and the tighter convergence criteria, except for R = 3.5 and 4.5 a.u.; those results were obtained with Molpro 2006 and the default convergence criteria. The H–H bond length is r = 1.449 a.u., the angle between the H_2 bond axis **r** and the pair-fixed z axis (along **R**) is θ, and the distance between the centers of mass of H_2 and H is R.

R	μ_x	μ_x(GMF)	μ_z	μ_z(GMF)
θ = 0°				
3.0	0	0	−0.068 855	−0.069 411
3.5	0	0	−0.034 992	−0.035 530
4.0	0	0	−0.011 906	−0.012 267
4.5	0	0	−0.001 161	−0.001 367
5.0	0	0	0.002 905	0.002 792
6.0	0	0	0.003 829	0.003 781
7.0	0	0	0.002 683	0.002 662
8.0	0	0	0.001 689	0.001 684
9.0	0	0	0.001 064	0.001 061
10.0	0	0	0.000 693	0.000 688
θ = 30°				
3.0	−0.014 908	−0.013 912	−0.092 080	−0.092 580
3.5	−0.010 327	−0.009 463	−0.050 876	−0.049 865
4.0	−0.007 211	−0.006 546	−0.022 959	−0.020 867
4.5	−0.005 195	−0.004 811	−0.008 620	−0.006 361
5.0	−0.003 811	−0.003 491	−0.002 064	−0.000 860
6.0	−0.002 101	−0.001 746	0.001 544	0.001 708
7.0	−0.001 194	−0.001 065	0.001 524	0.001 506
8.0	−0.000 708	−0.000 654	0.001 038	0.001 013
9.0	−0.000 442	−0.000 414	0.000 669	0.000 649
10.0	−0.000 290	−0.000 274	0.000 438	0.000 421
θ = 60°				
3.0	−0.012 731	−0.011 852	−0.143 668	−0.142 866
3.5	−0.009 222	−0.008 541	−0.081 857	−0.080 270
4.0	−0.006 677	−0.006 297	−0.043 229	−0.040 993
4.5	−0.004 907	−0.004 666	−0.022 026	−0.019 664
5.0	−0.003 638	−0.003 073	−0.011 002	−0.009 779
6.0	−0.002 025	−0.001 575	−0.002 654	−0.002 450
7.0	−0.001 156	−0.001 016	−0.000 662	−0.000 638
8.0	−0.000 689	−0.000 633	−0.000 210	−0.000 210
9.0	−0.000 430	−0.000 405	−0.000 101	−0.000 100
10.0	−0.000 282	−0.000 269	−0.000 063	−0.000 065
θ = 90°				
3.0	0	0	−0.170 623	−0.171 036
3.5	0	0	−0.096 544	−0.096 864
4.0	0	0	−0.052 405	−0.052 610
4.5	0	0	−0.028 028	−0.028 156
5.0	0	0	−0.015 011	−0.015 089
6.0	0	0	−0.004 580	−0.004 606
7.0	0	0	−0.001 690	−0.001 696
8.0	0	0	−0.000 805	−0.000 808
9.0	0	0	−0.000 473	−0.000 472
10.0	0	0	−0.000 308	−0.000 308

region around the nucleus in H_2 that is closer to the H atom gains a partial positive charge.

In Table II, we compare our results for the H_2–H dipole with *ab initio* results obtained previously by GFM,[20] with our results converted to the xz plane. The full comparison of the 288 values of μ_x or μ_z obtained in the calculations is provided in Tables S10–S14 of the supplementary material. The overall patterns of the dipole components are quite similar, but the several of the specific values differ. Comparing all 288 values from our work with the results of GFM,[20] we find an average difference of 27.5% between the two calculations. However, nine of the μ_z values are distinct outliers in terms of the magnitudes of the differences. In each of these cases, the geometrical configuration is close to the point where μ_z changes sign as R increases, at fixed θ. A slight displacement in the location of the R value where μ_z crosses zero leads to large percent differences. Excluding these nine points from the comparison set reduces the average absolute value of the discrepancy between our results and the earlier results[20] to 6.45%, a more realistic representation of the differences. The magnitude of the differences varies noticeably with the angle θ and the dipole component μ_x or μ_z. The closest agreement is found for μ_z with θ = 90°, where the percent difference is only 0.40%. In general, the differences in μ_z values are smaller than the differences in μ_x values. The averages of the absolute values of the percent differences in μ_z are 2.02% at 0° (excluding one outlier), 4.92% at 30° (excluding eight outliers), and 6.17% at 60°. The differences in the μ_x values are 8.91% at 30° and 10.2% at 60°.

As mentioned above, we have carried out two sets of calculations with larger basis sets, one with an aug-cc-pV6Z basis (A6Z) and the other with a d-aug-cc-pV5Z basis (D5Z). Results from these calculations for r = 1.449 a.u., eight R values, and 19 angles θ are listed in Table S15 in the supplementary material. The results from these larger basis sets agree well with the results from the aug-cc-pV5Z basis—the only exceptions are found very near to the points where μ_z changes sign. Yet even including those points, the absolute values of the results from the A6Z basis agree with the A5Z† results to ~0.25%, and the results from the D5Z basis agree with the A5Z† results to ~0.23%.

In two of the cases where the GFM results[20] and ours differ significantly, r = 1.449 a.u. and R = 5.0 a.u., with θ = 30° or θ = 60°, several additional independent calculations were run with Molpro 2015, the aug-cc-pV5Z basis, the tighter convergence criteria, and the base field strength f = 0.001 a.u. The results from RHF/RCCSD(T) and RHF/UCCSD(T) calculations are listed in Table III. Increasing f to 0.01 a.u. changed only the final digit in the values listed. The new calculations showed the same differences from GFM's results[20] as our previous work had shown.

Differences with the earlier results may be due to the choice of basis set and/or the computational method. The GFM calculations[20] were carried out in a Gaussian basis derived from the Huzinaga 10s basis,[250] augmented by p and d functions. The s functions with the three smallest exponents in the Huzinaga set[250] were placed at the center of the H_2 bond. The remaining seven s functions from the 10s basis were associated with each H nucleus individually, but the five with the largest exponents were contracted and then allowed to float off the protons. A set of p functions with exponent 1.2 was assigned to each H center, and p sets with exponents 0.3 and 0.1 were located at the bond center. Additionally, two sets of d functions with exponents 0.4 and 0.13 were located at the bond center. The basis used for the separate H atom itself is not explicitly specified in Ref. 20; however, if 3s, 2p, and 2d functions were placed at the midpoint of each H–H segment, and 3s and one set of p functions were assigned to each H center, this would give a total of 75 contracted functions in the basis, vs 165 in our work.

The earlier calculations were run in a multistep process, starting with self-consistent field (SCF) calculations, then generating localized orbitals from the molecular orbitals, in order to make it possible to separate intramolecular and intermolecular correlation.[251] Double excitations, from the $1\sigma_g^2$ configuration of H_2 obtained at the SCF level to $1\sigma_u^2$, $1\pi_u^2$, and $2\sigma_g^2$ configurations, were included to produce a multiconfigurational SCF (MCSCF) wave function. Then,

TABLE III. Calculated Cartesian dipole components (in a.u.) for two geometrical configurations of H_2–H. The bond length of H_2 is r = 1.449 a.u., and the separation between the centers of mass of H_2 and H is R = 5.0 a.u. along the z axis in both cases. The angle between the H_2 bond axis and the z axis is θ. Results from different *ab initio* methods and implementations are listed. The base field f is described in the text.

θ = 30°	Wave function	Base field	μ_x	μ_z
GFM			−0.003 491	−0.000 860
Molpro 2006	RHF/UCCSD(T)	f = 0.002	−0.003 811	−0.002 065
Molpro 2012	RHF/UCCSD(T)	f = 0.002	−0.003 811	−0.002 064
Molpro 2015	RHF/RCCSD(T)	f = 0.001	−0.003 810	−0.002 022
	RHF/UCCSD(T)	f = 0.001	−0.003 811	−0.002 064
θ = 60°	Wave function	Base field	μx	μz
GFM			−0.003 073	−0.009 779
Molpro 2006	RHF/UCCSD(T)	f = 0.002	−0.003 638	−0.011 002
Molpro 2012	RHF/UCCSD(T)	f = 0.002	−0.003 638	−0.011 002
Molpro 2015	RHF/RCCSD(T)	f = 0.001	−0.003 637	−0.010 969
	RHF/UCCSD(T)	f = 0.001	−0.003 638	−0.011 002

all single and double excitations from the MCSCF function were included in the coupled-electron pair approximation (CEPA), which is size consistent.[20,251] To minimize basis-set superposition errors, in previous calculations for H_2 interacting with an inert gas atom, intra-H_2 correlation had been treated separately from the correlations between electrons in orbitals localized to H_2 and electrons in orbitals localized on the inert gas atom. The separation of correlation effects was implemented via the self-consistent coupled electron pair (SCEP) technique.[20,251] This approach has yielded highly accurate results for the interaction-induced dipoles of H_2–He[158,159,161] and H_2–H_2.[251] Our previous work on the collision-induced dipole of H_2–He at the CCSD(T) level[169] gave results for the Cartesian dipole components that agreed very well with those of Borysow, Frommhold, and Meyer.[164] It is possible that differences between the wave function obtained in Ref. 20 and our RHF/UCCSD(T) function contribute to the observed differences in the dipole components for the open-shell system H_2–H.

The breakdown of the Hellmann-Feynman theorem[26,252–254] for various approximate wave functions[255] means that the dipole obtained as an expectation value need not agree exactly with the dipole obtained from finite-field calculations. In general, the error in the expectation value of the dipole moment is of first-order in the error in the wave function, while the error in the energy is of second-order in the error in the wave function. This may make the finite-field results preferable.[256]

III. SPHERICAL TENSOR ANALYSIS

For applications in computing line shapes for collision-induced spectra, the calculated dipole needs to be represented as a series in the spherical harmonics of the orientation angles Ω_r and Ω_R for the bond axis **r** and the intermolecular vector **R**, respectively,[22–25]

$$\mu^M = 4\pi/3^{1/2} \sum_{\lambda,L,m} D_{\lambda L}(r,R) Y_\lambda{}^m(\Omega_r) Y_L{}^{M-m}(\Omega_R) \langle \lambda\, m\, L\, M-m | 1\, M\rangle. \quad (1)$$

In this equation, M designates the spherical-tensor component of the dipole. The M = 0 component is identical to μ_z, $\mu^{+1} = -(1/2)^{1/2}(\mu_x + i\mu_y)$, and $\mu^{-1} = (1/2)^{1/2}(\mu_x - i\mu_y)$. The values of $D_{\lambda L}(r, R)$ depend only on λ, L, and the magnitudes of r and R. The quantity $\langle \lambda\ m\ L\ M - m|1M\rangle$ is a Clebsch-Gordan coefficient. Due to the symmetry of the H_2 molecule, λ is always even, and for the Clebsch-Gordan coefficient to be nonzero, $L = \lambda \pm 1$. Also, because **R** is oriented along the z axis, M − m = 0.

The coefficients $D_{\lambda L}(r, R)$ have been determined by least-squares fits to the Cartesian components of the dipole moment as functions of the orientation angle θ of H_2, at fixed r and R. We fit the 17 nonzero values of μ_y for the various angles θ, together with all 19 values of μ_z. In the first study, dipole coefficients through λ = 24 and L = 25 were determined from the Cartesian dipole components. The coefficients beyond $D_{89}(r, R)$ are virtually negligible for $r \le 1.787$ a.u. For r = 2.125 a.u.–2.801 a.u., the higher coefficients start to grow at small R values, but they are still substantially smaller than the leading coefficients. Also, the higher coefficients tend to be erratic as functions of R, suggesting that while they do help to determine a least-squares fit to the data, they are not physically meaningful. In the second set of calculations, we fit the coefficients $D_{\lambda L}(r, R)$ only through $D_{89}(r, R)$. In Table IV, we list the coefficients $D_{01}(r, R)$, $D_{21}(r, R)$, $D_{23}(r, R)$, $D_{43}(r, R)$, $D_{45}(r, R)$, $D_{65}(r, R)$, $D_{67}(r, R)$, $D_{87}(r, R)$, and $D_{89}(r, R)$ for r = 1.449 a.u. as obtained from fits to both sets of results with the A5Z basis, from a fit through D_{89} to the results from the A6Z basis and from a fit through D_{89} to the results from the D5Z basis. The A5Z results for the coefficients $D_{\lambda L}(r, R)$ over the full range of r values from r = 0.942 a.u. to r = 2.801 a.u. are listed in Tables S16–S24 of the supplementary material. The dipole coefficients from the second set of A5Z calculations (with tighter convergence criteria) are indicated by a superscript †. Generally, the values of the coefficients from D_{01} to D_{89} from all four sets of calculations at r = 1.449 a.u. and from the two sets of calculations at the other r values agree well. This is noteworthy, considering that the first set of results comes from fits up to λ = 24 and L = 25, while in the second, third, and fourth sets, no dipole coefficients beyond D_{89} were included. The differences indicate the level of uncertainty in the results. The coefficient D_{23} appears to be best determined overall; relative to the A5Z† results, the average absolute value of the difference in the A5Z results is 0.064%; for the A6Z results, 0.11%; and for the D5Z results, 0.14%. Excluding the range from R = 8.0 a.u. to R = 10.0 a.u. (where D_{01} is typically single-digit), the average absolute value of the difference in D_{01} relative to A5Z† is 0.011% for A5Z, 0.16% for A6Z, and 1.57% for D6Z. Differences in D_{21} among the results with different basis sets are less than 1%; differences in D_{45} are less than 2%, and differences in D_{43} are less than 3% (again, excluding R values where the coefficients are single-digit).

Results for the dipole coefficients D_{01}, D_{21}, D_{23}, D_{43}, and D_{45} based on the work of GFM[20] are also listed in Table IV and in Tables S16–S24. These values were obtained from a least-squares fit of the dipole coefficients $D_{\lambda L}$ to the Cartesian dipole components reported in Ref. 20. The *ab initio* calculations in Ref. 20 gave a total of 6 nonzero Cartesian dipole components, from which we have derived the coefficients up to D_{45}. From the tables, the dipole coefficients obtained from Ref. 20 agree reasonably well with our results in terms of the overall pattern of the coefficients, but in terms of the numerical values, discrepancies with Ref. 20 are evident in cases where the results from our four basis sets (A5Z, A5Z†, A6Z, and D5Z) agree well. We have carried out further calculations to separate effects on the dipole coefficients $D_{\lambda L}(r, R)$ that are due to differences in the Cartesian components of the dipoles vs the effects of working with four angles in Ref. 20 and 19 angles in the current study. We determined the dipole coefficients D_{01}, D_{21}, D_{23}, D_{43}, and D_{45} from the Cartesian dipole components in the A5Z† calculations but restricted to the angles 0°, 30°, 60°, and 90°. These results are listed on the lines labeled (45) in Tables IV and S16–S24. The results from the (45) fits are generally quite close to the results from the full 19-angle fits, and they are closer to those results than to the earlier results from Ref. 20. Our results suggest that the leading dipole coefficients can usually be determined quite well from calculations at a smaller number of angles.

In Fig. 5, we plot D_{01}, D_{21}, D_{23}, D_{43}, and D_{45} vs the H_2–H separation R, for bond length r = 1.449 a.u., to show how the magnitudes of the coefficients compare. For small R, the isotropic overlap and exchange coefficient D_{01} is larger in magnitude than all of the other coefficients, and it is negative. The crossover of $|D_{01}|$ with D_{23} occurs between R = 5.0 a.u. and 6.0 a.u. In Fig. 6, we show D_{01}, D_{21}, D_{23}, D_{43}, and D_{45} vs R for r = 2.125 a.u. The coefficients are generally larger

TABLE IV. Coefficients for the spherical harmonic expansion of the dipole of H_2–H in Eq. (1). Results in a.u. multiplied by 10^6 are listed as obtained with the A5Z basis and the default convergence criteria, with the A5Z basis and tighter convergence criteria (indicated by a superscript †), with the A6Z basis, and with the D5Z basis. Results from a fit limited to θ = 0°, 30°, 60°, and 90° are listed in the rows labeled (45), for the most direct comparison with the results of GFM.[20] The H_2 bond length is 1.449 a.u.

R (a.u.)	D_{01}	D_{21}	D_{23}	D_{43}	D_{45}	D_{65}	D_{67}	D_{87}	D_{89}
3.0†	−135 447	−10 736	31 156	1079	59	121	−80	2	−2
A6Z	−135 448	−10 740	31 150	1079	56	119	−79	2	−2
D5Z	−135 455	−10 733	31 150	1082	57	118	−80	2	−4
(45)	−135 421	−10 687	31 100	1144	6				
GFM	−135 348	−11 260	30 574	1281	−217				
3.4	−86 532	−5 943	21 022	248	466	56	−22	3	−2
3.5	−76 474	−5 269	19 272	138	486	44	−14	3	−2
(45)	−76 466	−5 254	19 257	162	471				
GFM	−75 599	−5 914	19 070	576	−100				
3.6	−67 364	−4 697	17 716	55	490	34	−8	2	−1
3.7	−59 173	−4 201	16 319	−8	483	25	−3	2	−1
3.8	−51 853	−3 764	15 055	−51	467	20	−1	1	−1
3.9	−45 342	−3 372	13 905	−84	449	13	3	2	−1
4.0	−39 575	−3 019	12 853	−103	425	10	4	2	0
4.0†	−39 575	−3 019	12 853	−102	425	10	4	2	0
A6Z	−39 581	−3 026	12 848	−104	422	8	3	0	0
D5Z	−39 584	−3 021	12 849	−104	425	7	2	1	2
(45)	−39 574	−3 017	12 852	−98	424				
GFM	−38 087	−3 649	12 984	482	−392				
4.5	−19 590	−1 686	8 744	−113	295	1	7	2	0
(45)	−19 588	−1 687	8 746	−113	296				
GFM	−17 976	−2 214	9 002	516	−492				
5.0	−9 378	−890	6 022	−78	190	−2	4	1	1
5.0†	−9 378	−890	6 023	−78	189	−2	4	1	1
A6Z	−9 381	−894	6 020	−77	189	−2	4	0	0
D5Z	−9 378	−890	6 018	−78	190	0	4	1	0
(45)	−9 379	−891	6 024	−79	191				
GFM	−8 538	−1 384	5 992	347	−141				
6.0	−1 903	−219	3 004	−25	74	0	1	0	1
6.0†	−1 904	−219	3 004	−26	74	0	2	1	1
A6Z	−1 903	−221	3 002	−25	74	−1	1	0	0
D5Z	−1 892	−217	2 999	−25	73	0	2	1	0
(45)	−1 904	−219	3 004	−26	74				
GFM	−1 778	−516	2 813	61	32				
7.0	−279	−51	1 622	−7	30	1	1	0	0
7.0†	−279	−51	1 622	−7	30	1	1	1	0
A6Z	−277	−51	1 620	−8	30	0	1	0	0
D5Z	−259	−49	1 621	−5	30	1	0	0	0
(45)	−279	−51	1 622	−7	30				
GFM	−276	−137	1 546	1	28				
8.0	6	−12	942	−2	14	1	1	0	0
8.0†	6	−12	942	−2	14	1	1	0	0
A6Z	9	−12	942	−2	13	0	0	0	0
D5Z	27	−12	945	−1	13	0	0	0	0
(45)	6	−12	942	−2	13				
GFM	−2	−45	909	−4	17				

TABLE IV. (*Continued.*)

R (a.u.)	D_{01}	D_{21}	D_{23}	D_{43}	D_{45}	D_{65}	D_{67}	D_{87}	D_{89}
9.0	25	−5	586	−1	8	0	1	0	1
9.0†	31	−4	585	0	7	1	0	0	0
A6Z	32	−4	583	−1	7	0	0	0	0
D5Z	46	−5	586	0	7	1	0	0	0
(45)	31	−5	585	0	7				
GFM	26	−18	567	−3	8				
10.0	13	−1	383	0	4	0	1	−1	1
10.0†	22	−2	382	1	3	0	0	0	0
A6Z	21	−1	381	0	3	0	0	0	0
D5Z	32	−4	383	1	3	0	0	0	0
(45)	22	−2	382	1	4				
GFM	16	−8	371	−2	5				

at 2.125 a.u., and D_{43} and D_{45} become noticeably different from zero on the same plot with the other coefficients.

Long-range classical induction effects are reflected in D_{23} for quadrupolar induction and D_{45} for hexadecapolar induction.[22–25] Through order R^{-7}, D_{23} is the sum of a direct quadrupolar induction term that varies as R^{-4} and an R^{-7} back-induction term. From Ref. 23, for an atom A and molecule B, through order R^{-7} at long range,

$$D_{23}(r,R) = 3^{1/2}\alpha_A\Theta_B(r)R^{-4} + 3^{1/2}(4/35)[3\,\alpha_{B,zz}(r) + 4\,\alpha_{B,xx}(r)]\alpha_A\Theta_B(r)R^{-7}, \quad (2)$$

where α_A is the polarizability of the atom, $\Theta_B(r)$ is the quadrupole of the molecule as a function of bond length r, $\alpha_{B,zz}(r)$ is the molecular polarizability parallel to the bond axis as a function of r, and $\alpha_{B,xx}(r)$ is the polarizability perpendicular to the bond axis. The quadrupole of H_2 and the components of the polarizability of H_2 are known accurately at the specific r values used here, from the work of Miliordos and Hunt.[257] The polarizability of the H atom is $\alpha_H = 4.5$ a.u. In Fig. 7, we show that $D_{23}(r, R)$ converges to the quadrupolar induction form as R increases, for bond lengths r = 1.111 a.u., r = 1.449 a.u., and r = 1.787 a.u. Results for other bond lengths are similar. In Table V, we list the values of the quadrupole that would be deduced from $D_{23}(r, R)$ at R = 8.0, 9.0, and 10.0 a.u. for each bond length r, if the coefficient were entirely due to quadrupolar induction. At shorter range, the values of $D_{23}(r, R)$ reflect overlap damping of the classical induction effects, as well as exchange and orbital distortion, which tend to reduce $D_{23}(r, R)$ from its long-range limiting form. Two estimates of the quadrupole are shown for each r value, the first (a) obtained with the R^{-4} term in Eq. (2) alone and the second (b) from the full version of Eq. (2), with *ab initio* values used for the polarizability components.[257] Agreement with the quadrupole values that have been calculated *ab initio*[257] is very good, and the agreement improves as R increases, as shown in Fig. S2 in the supplementary material. The average error in the value of Θ derived from $D_{23}(r, R)$ at R = 10.0 a.u. is 1.20%, when the R^{-7} back-induction term is included in the analysis. The estimated quadrupole is always larger than the *ab initio* quadrupole.

The coefficient $D_{45}(r, R)$ is determined by hexadecapolar induction at long range. For an atom A and molecule B, to leading order,[22–25]

$$D_{45}(r,R) = 5^{1/2}\alpha_A\Phi_B(r)R^{-6}, \quad (3)$$

where $\Phi_B(r)$ denotes the hexadecapole of the molecule as a function of bond length. In Fig. 8, we show that $D_{45}(r, R)$ from our calculations converges to the known hexadecapolar induction form for

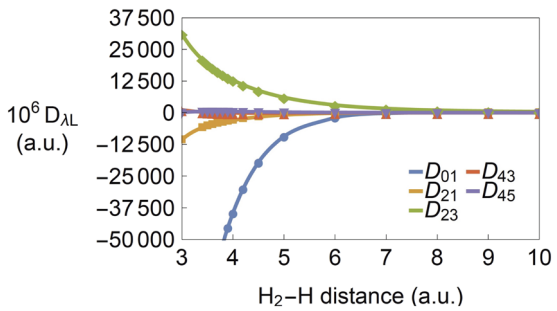

FIG. 5. Dipole coefficients D_{01}, D_{21}, D_{23}, D_{43}, and D_{45} for H_2–H as functions of R for r = 1.449 a.u.

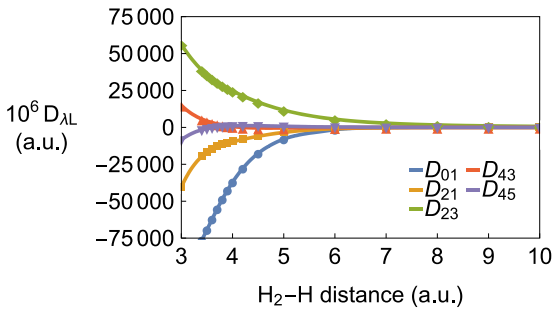

FIG. 6. Dipole coefficients D_{01}, D_{21}, D_{23}, D_{43}, and D_{45} for H_2–H as functions of R for r = 2.125 a.u.

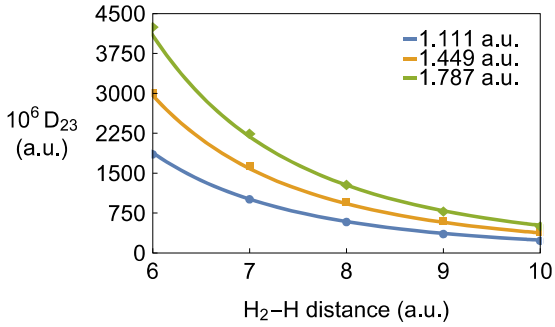

FIG. 7. Dipole coefficients D_{23} as functions of R, showing convergence of the *ab initio* values to the quadrupolar induction form at long range, for bond lengths r = 1.111, 1.449, and 1.787 a.u.

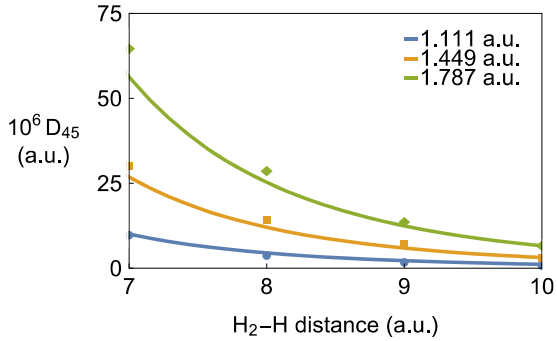

FIG. 8. Dipole coefficients D_{45} as functions of R, showing convergence of the *ab initio* values to the hexadecapolar induction form at long range, for bond lengths r = 1.111, 1.449, and 1.787 a.u.

r = 1.111 a.u., r = 1.449 a.u., and r = 1.787 a.u. Results for other r values are similar, except for r = 0.942, where the hexadecapole is quite small. Hexadecapolar induction effects were not detectable in the study of the interaction-induced dipole of H_2–H in Ref. 20. In Table VI, we compare the values of the hexadecapole as a function of bond length deduced from D_{45}(r, R) at R = 8.0, 9.0, and 10.0 a.u. with the values that have been computed directly *ab initio*. Figure S3 in the supplementary material shows that the agreement increases with increasing R. The difference between the *ab initio* values of Φ[257] and the estimates of Φ based on D_{45}(r, R) at R = 10.0 a.u. is 40% for r = 0.942 a.u. and 9.5% for 1.111 a.u.; for the other bond lengths, the percent error in the hexadecapole estimated from D_{45}(r, R) at R = 10.0 a.u. ranges from 4.7% to 7.2%. The estimated hexadecapole is always larger than the *ab initio* hexadecapole for r ≥ 1.280 a.u.

At long range, the coefficient D_{01}(r, R) is determined by van der Waals dispersion and back-induction;[23] it varies as R^{-7} to leading order. The polarization of the electronic charge distribution on each center (H_2 or H) due to the H_2–H interaction attracts the nuclei on the same center.[26] The van der Waals dispersion force between two atoms in S states was explained by Feynman as a result of this electrostatic attraction.[26] Hunt later proved Feynman's "conjecture" analytically and proved that it also holds for molecules of arbitrary symmetry.[32] Electron correlation allows electronic charge to accumulate between the nuclei, but the dispersion forces on the nuclei themselves are classical electrostatic forces.[26,32]

The dispersion dipole is derived from the change in dispersion energy for interacting molecules in a uniform applied electric field. The electric field alters the interaction energy in two ways: Each molecule is hyperpolarized by the concerted effects of the applied field and the fluctuating field from the neighboring molecule.[31] Additionally, the applied field alters the correlations of the spontaneously fluctuating charge densities on each center.[31]

Perturbation analyses of the dispersion dipole have been presented by Byers Brown and Whisnant[27] and by Craig and Thirunamachandran.[30] Hunt developed an approximation for the dispersion dipole in terms of static polarizabilities α and dipole-dipole quadrupole polarizabilities B of the interacting molecules, along with the C_6 van der Waals coefficient for the pair.[28] Subsequently, Galatry

TABLE V. Quadrupole moments (in a.u.) estimated from D_{23}(r, R) compared with quadrupole moments Θ^{calc} calculated *ab initio*.[257] The tabulated D_{23} values have been multiplied by 10^6. The estimate Θ^{est}(a) is obtained by considering only the direct quadrupolar induction contribution to D_{23}(r, R) of order R^{-4}, while Θ^{est}(b) also includes back-induction effects of order R^{-7}. The calculated quadrupole at r = 1.618 a.u. has been obtained by interpolation of the results in Ref. 257, as have the polarizability tensor components at r = 1.618 a.u. needed to obtain Θ^{est}(b).

	R = 8.0 (a.u.)			R = 9.0 (a.u.)			R = 10.0 (a.u.)			
r (a.u.)	D_{23}	Θ^{est}(a)	Θ^{est}(b)	D_{23}	Θ^{est}(a)	Θ^{est}(b)	D_{23}	Θ^{est}(a)	Θ^{est}(b)	Θ^{calc}
0.942	446.1	0.2344	0.2332	277.6	0.2337	0.2328	182.2	0.2338	0.2331	0.2302
1.111	599.5	0.3150	0.3130	373.1	0.3140	0.3126	244.6	0.3137	0.3127	0.3086
1.280	766.2	0.4027	0.3997	476.4	0.4011	0.3990	312.0	0.4004	0.3989	0.3934
1.449	942.2	0.4951	0.4909	584.8	0.4923	0.4893	382.4	0.4907	0.4885	0.4823
1.618	1123.0	0.5902	0.5843	695.3	0.5853	0.5812	454.1	0.5825	0.5795	0.5729
1.787	1303.8	0.6852	0.6774	805.0	0.6776	0.6723	525.0	0.6735	0.6696	0.6624
2.125	1642.9	0.8634	0.8513	1008.3	0.8488	0.8404	655.7	0.8412	0.8351	0.8266
2.463	1911.7	1.0047	0.9880	1165.5	0.9811	0.9696	755.6	0.9694	0.9611	0.9507
2.801	2063.7	1.0845	1.0643	1248.0	1.0506	1.0368	806.3	1.0344	1.0244	1.0126

TABLE VI. Hexadecapole moments (in a.u.) estimated from $D_{45}(r, R)$ compared with hexadecapole moments Φ^{calc} calculated *ab initio*.[257] The tabulated D_{45} values have been multiplied by 10^6. The estimate Φ^{est} is obtained from the direct hexadecapolar induction contribution to $D_{45}(r, R)$ of order R^{-6}. The calculated hexadecapole at r = 1.618 a.u. has been obtained by interpolation of the results in Ref. 257.

	R = 8.0 (a.u.)		R = 9.0 (a.u.)		R = 10.0 (a.u.)		
r (a.u.)	D_{45}	Φ^{est}	D_{45}	Φ^{est}	D_{45}	Φ^{est}	Φ^{calc}
0.942	1.83	0.05	0.99	0.05	0.38	0.04	0.0628
1.111	4.39	0.11	2.31	0.12	1.07	0.11	0.1175
1.280	8.52	0.22	4.34	0.23	2.10	0.21	0.1993
1.449	13.77	0.36	6.81	0.36	3.36	0.33	0.3139
1.618	20.50	0.53	9.91	0.52	4.97	0.49	0.4664
1.787	29.13	0.76	13.89	0.73	7.00	0.70	0.6582
2.125	52.15	1.36	24.65	1.30	12.42	1.23	1.1649
2.463	83.19	2.17	38.58	2.04	19.36	1.92	1.8052
2.801	117.46	3.06	53.74	2.84	26.88	2.67	2.4912

and Gharbi[29] derived an exact expression for the dispersion dipole of a pair of atoms A and B in terms of the integrals of $\alpha^A(i\omega)$ $B^B(0, i\omega)$ and $\alpha^B(i\omega)$ $B^A(0, i\omega)$ over imaginary frequencies. Bohr and Hunt carried out a symmetry analysis to find the dispersion contributions to D_{01}, D_{21}, D_{23}, and D_{43} for an atom A interacting with molecule B;[23] the dispersion contribution to D_{45} vanishes.[23] Combining the dispersion term in D_{01} with the back-induction effect[23] gives

$$D_{01}(r, R) = (9\hbar/\pi)R^{-7}\int_0^\infty \left[\alpha^A(i\omega)\tilde{B}^B(0, i\omega) - \tilde{\alpha}^B(i\omega)B^A(0, i\omega)\right]d\omega + (6/5)[\alpha_{B,zz}(r) - \alpha_{B,xx}(r)]\alpha_A\Theta_B(r)R^{-7}, \quad (4)$$

where

$$\tilde{B}^B(0, i\omega) = (2/15)\left[B^B{}_{zz,zz}(0, i\omega) + 2B^B{}_{xz,xz}(0, i\omega) + 2B^B{}_{zx,xz}(0, i\omega) + B^B{}_{xx,zz}(0, i\omega) + 4B^B{}_{xx,xx}(0, i\omega)\right] \quad (5)$$

and

$$\tilde{\alpha}^B(i\omega) = (1/3)\left[\alpha^B{}_{zz}(i\omega) + 2\alpha^B{}_{xx}(i\omega)\right]. \quad (6)$$

The integrals in Eq. (4) have been evaluated very accurately for H_2–H by Bishop and Pipin, using explicitly correlated wave functions for H_2 and an H_2 bond length r of 1.449 a.u.[34]

The coefficient $D_{01}(r, R)$ typically changes sign with increasing H_2–H separation near R = 8.0 a.u., where there are still substantial exchange/overlap contributions to $D_{01}(r, R)$. Therefore, in order to make comparisons with the known long-range analytical form of $D_{01}(r, R)$ as a function of R for $r = r_0 = 1.449$ a.u., we have determined $D_{01}(r_0, R)$ for R = 10.0–15.0 a.u. in intervals of 1.0 a.u. Placing H_2–H in the yz plane, we calculated the dipole in the y and z directions at angles θ = 0°, 15°, 30°, 45°, 60°, 75°, and 90° using a base field strength f = 0.01 a.u. and the A5Z basis and then determined the coefficients D_{01}, D_{21}, D_{23}, D_{43}, and D_{45} from the results. We have found that corrections for the basis set superposition error (BSSE)[258] are small with basis sets of the size used here, in previous work on interaction effects on the polarizability of H_2–H_2.[172] At very long range, however, the collision-induced dipole is quite small, and the BSSE corrections become appreciable relative to the values of the dipole. Values of $D_{01}(r_0, R)$ obtained with and without BSSE corrections are given in Table S25. A log-log plot of D_{01} vs R in the range from 10.0 to 15.0 a.u. has a slope of −6.06, based on values without BSSE corrections. When the BSSE corrections are added, the slope is −7.31, vs the expected value −7 at very long range. The dispersion contribution to D_{01} for H_2–H at r = 1.449 a.u. is 186.39 R^{-7} from the work of Bishop and Pipin.[34] The back-induction contribution is appreciably smaller at 5.17 R^{-7}, based on α_{zz} = 6.7179 a.u., α_{xx} = 4.7319 a.u., Θ = 0.4823 a.u. (from Ref. 257), and α^H = 4.5 a.u. Figure 9 shows the *ab initio* results for D_{01} with BSSE corrections vs R for r = 1.449 a.u. compared with the analytical long-range form. The level of agreement is striking, given the challenges in obtaining accurate values for this numerically sensitive property.

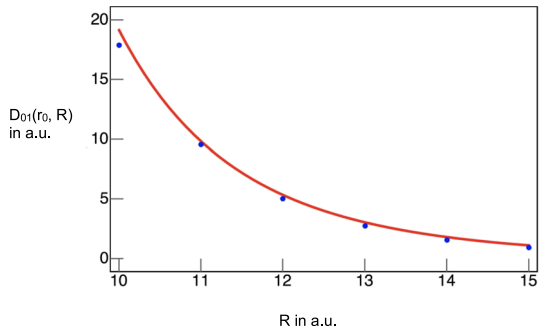

FIG. 9. Dipole coefficient $D_{01}(r_0, R)$ as a function of R, for bond length r_0 = 1.449 a.u. Points plotted in blue are the *ab initio* results with BSSE corrections. The red curve shows the accurate R^{-7} term in D_{01} due to van der Waals dispersion and back-induction.

IV. DISCUSSION AND COMPARISON WITH THE DIPOLE OF H_2–He

The results from both full sets of calculations for the Cartesian components of the dipole moment with an aug-cc-pV5Z basis set are given in Tables S1–S9 of the supplementary material, for H_2 bond lengths of 0.942 through 2.801 a.u., for separations R between the centers of mass of H_2 and H from 3.0 a.u. to 10.0 a.u., and for the angle θ between the H_2 bond vector **r** and the vector **R** from the center of mass of H_2 to the nucleus of the H atom ranging from 0° to 90° in intervals of 5°. The H_2–H system lies in the yz plane and R points along z, with y to the right. In general, the results obtained with the default convergence criteria agree very well with the results obtained with tighter convergence criteria, marked with a superscript †. Differences are observed in some cases where the dipole is small, either where R is large or where the dipole function crosses zero as R increases. In those cases, the results obtained with the tighter convergence criteria are to be preferred. Cartesian components of the dipole are compared in detail with the results from Ref. 20 in Tables S10–S14. Table S15 compares components of the dipole obtained with the aug-cc-pV5Z, aug-cc-pV6Z, and d-aug-cc-pV5Z basis sets, for r = 1.449 a.u.

In Tables S16–S24, the results from multiple sets of calculations for the spherical-tensor dipole coefficients D_{01}, D_{21}, D_{23}, D_{43}, D_{45}, D_{65}, D_{67}, D_{87}, and D_{89} are listed. Again, the results obtained with the tighter convergence criteria (marked by †) should be considered more accurate when the results differ. The results obtained by truncating the series in Eq. (1) at the D_{89} term (in the calculations marked by †) generally agree quite well with the results obtained by continuing the series to $D_{\lambda L}$ with λ = 24 and L = 25, in the original calculations where the default convergence criteria were used. Differences are apparent between the $D_{\lambda L}$ coefficients derived from the values of the Cartesian components of the dipole in Ref. 20 vs our values. By contrast, the results for D_{01}, D_{21}, D_{23}, D_{43}, and D_{45} obtained from our Cartesian dipole components at angles θ = 0°, 30°, 60°, and 90° agree rather well with the results from the full set of angles in this work. The results from the four-angle fits are listed in Tables S16–S24 in the rows labeled (45).

Recent work by Miliordos and Hunt[257] has given the polarizability tensor components, the quadrupole moment, and the hexadecapole moment of H_2 at the specific bond lengths used in this work, except for r = 1.618 a.u. The values of α_{zz} and α_{xx} in Ref. 257 agree well earlier calculations of the polarizability of H_2[259–262] and show quite close agreement with interpolated values based on the work of Rychlewski[261] and of Raj, Hamaguchi, and Witek.[262] The quadrupoles agree well with interpolated values based on earlier accurate work,[263–265] and similarly the hexadecapoles agree well with interpolated values based on accurate calculations completed earlier.[263–265] With the values from Ref. 257, we have confirmed the convergence of D_{23} and D_{45} from our calculations to the known long-range forms, the first time this has been observed for the hexadecapolar induction term D_{45}. Convergence of D_{23} and D_{45} to the long-range forms has been found for each of the bond lengths in this work, except for D_{45} at r = 0.942 or 1.111 a.u. where the hexadecapole is quite small.

The coefficient D_{01} gives the contribution to the dipole that is isotropic in the orientation of H_2. At short range where D_{01} reflects overlap and exchange effects as well as dispersion, D_{01} is negative. At long range, both the long-range dispersion contribution to D_{01} and the much smaller back-induction contribution are positive. After correcting for basis set superposition error, we have obtained good agreement with the leading term in the long-range series for D_{01}, as shown in Fig. 9.

A comparison of the results for H_2–H with those for H_2–He shows that D_{23} and D_{45} are positive in both cases, as expected. For bond lengths r = 1.111, 1.449, and 1.787 a.u., we have confirmed that the ratio of D_{23} for H_2–H to D_{23} for H_2–He converges at large R values to the ratio of the polarizabilities of H and He, 4.5/1.383, as expected. The convergence is illustrated in Fig. S4 in the supplementary material. Figure S5 in the supplementary material shows that the ratio of D_{45} for H_2–H to D_{45} for H_2–He converges to the ratio of H and He polarizabilities for r = 1.449, 1.787, and 2.125 a.u. For R < 7.0 a.u., both ratios drop below the long-range limits and both become smaller as R decreases, showing that overlap effects on D_{23} and D_{45} are greater for H_2–H than for H_2–He.

The most striking difference between the dipoles of H_2–H and H_2–He is found for the coefficient D_{01}. As noted above, D_{01} is negative at short range for H_2–H and positive at long range, indicating that the polarity averaged over H_2 orientations corresponds to $H_2^{\delta+}H^{\delta-}$ at short range—where overlap and exchange effects predominate—and to $H_2^{\delta-}H^{\delta+}$ at long range—where the van der Waals dispersion term is most significant. By contrast, for H_2–He, D_{01} is positive at short range and negative at long range, so after averaging over the orientations of H_2, the polarity is $H_2^{\delta-}He^{\delta+}$ at short range and $H_2^{\delta+}He^{\delta-}$ at long range. The signs of D_{01} at long range obtained from the *ab initio* results in this work and earlier work on the H_2–He dipole agree with the signs of the dispersion dipole calculated directly by Bishop and Pipin[34] for H_2–H and H_2–He. In both cases, $D_{23} > D_{01}$ at long range, but $|D_{01}| > D_{23}$ at short range. The crossover of $|D_{01}|$ and D_{23} occurs for R values somewhat smaller than R_e, the location of the potential minima. The coefficients D_{21} and D_{43}, which carry information about the anisotropic overlap effects on the dipole, have the same signs for H_2–H and H_2–He.

Our earlier results for the interaction-induced dipoles of H_2–H_2 and H_2–He[169] at the CCSD(T) level in an aug-cc-pV5Z basis have been used to calculate the binary collision-induced absorption spectra for H_2 gas and to determine infrared and far infrared absorption during H_2–He collisions in an H_2/He mixture, over a range of temperatures.[180,181] Excellent agreement with experimental measurements from 77 K to 300 K has been found in both cases.[169,180,181] The calculations in this work on H_2–H have been carried out with basis sets of similar size, at the UCCSD(T) level for the wave function. While the open-shell character of H_2–H causes differences from the earlier work, we expect the values of the dipole moment presented here to be comparable in accuracy to our results for the H_2–H_2 and H_2–He dipoles.[169,180,181]

SUPPLEMENTARY MATERIAL

Tables S1–S9 give the interaction-induced dipole moments μ_y and μ_z from the first and second set of calculations for H_2 bond lengths r of 0.942, 1.111, 1.280, 1.449, 1.618 (second set only), 1.787, 2.125, 2.463, and 2.801 a.u., for angles θ from 0° to 90°, and for separations R between the centers of mass of H_2 and H from 3.0 a.u.

to 10.0 a.u. Default convergence criteria were used in the first set of calculations, and tighter convergence criteria were used in the second set (marked by †). In Tables S10–S14, our Cartesian dipole components are compared with the results obtained in Ref. 20, and in Table S15, Cartesian dipole components obtained with aug-cc-pV5Z, aug-cc-pV6Z, and d-aug-cc-pV5Z basis sets are compared for r = 1.449 a.u., the averaged internuclear distance in the ground rovibrational state of H_2. Tables S16–S24 list the spherical tensor expansion coefficients D_{01}, D_{21}, D_{23}, D_{43}, D_{45}, D_{65}, D_{67}, D_{87}, and D_{89} from our two full calculations, along with D_{01}, D_{21}, D_{23}, D_{43}, and D_{45} from the work of GFM[20] and from our calculations at $\theta = 0°$, 30°, 60°, and 90°. Table S25 lists the values of $D_{01}(r, R)$ for r = 1.449 a.u. and R from 10.0 to 15.0 a.u. as obtained from calculations with and without corrections for basis set superposition error. The dependence of the Cartesian components of the dipole on r, R, and θ is discussed in detail in a section of the supplementary material. In Fig. S1, the dipole component μ_z is plotted vs θ and R at r = 1.449 a.u., for $\Delta E/k_B$ less than or equal to 30 K, 300 K, 750 K, 1050 K, and 2600 K, where ΔE is the difference between the energy of a specific configuration and the minimum on the potential energy surface. In Figs. S2 and S3, we show that the quadrupoles and hexadecapoles derived from $D_{23}(r, R)$ and $D_{45}(r, R)$, respectively, converge to the *ab initio* values with increasing R, for the various bond lengths in this work. A plot of the ratios of D_{23} for H_2–H to D_{23} for H_2–He vs R for r = 1.111, 1.449, and 1.787 a.u. is included, along with a plot of the ratios of D_{45} for H_2–H to D_{45} for H_2–He, for r = 1.449, 1.787, and 2.125 a.u.

ACKNOWLEDGMENTS

This research was supported in part by NSF Grant No. 1300063 from the program in Chemical Theory, Models, and Computational Methods. E.M. is indebted to Auburn University for financial support of this research. Part of the calculations reported here were completed with resources provided by the Auburn University Hopper Cluster.

REFERENCES

[1] *Phenomena Induced by Intermolecular Interactions*, NATO ASI Series B, edited by G. Birnbaum (Plenum, New York, 1985), Vol. 127.
[2] *Collision-and Interaction-Induced Spectroscopy*, NATO ASI Series C, edited by G. C. Tabisz and M. N. Neuman (Kluwer, Dordrecht, 1995), Vol. 452.
[3] L. Frommhold, *Collision-Induced Absorption in Gases* (Cambridge University Press, Cambridge, England, 2006).
[4] J.-M. Hartmann, C. Boulet, and D. Robert, *Collisional Effects on Molecular Spectra: Laboratory Experiments and Models, Consequences for Applications* (Elsevier, Amsterdam, 2008).
[5] J.-M. Hartmann, H. Tran, R. Armante, C. Boulet, A. Campargue, F. Forget, L. Gianfrani, I. Gordon, S. Guerlet, M. Gustafsson, J. T. Hodges, S. Kassi, D. Lisak, F. Thibault, and G. C. Toon, J. Quant. Spectrosc. Radiat. Transfer **213**, 178 (2018).
[6] P. Siegbahn and B. Liu, J. Chem. Phys. **68**, 2457 (1978).
[7] W. Cencek and J. Rychlewski, J. Chem. Phys. **98**, 1252 (1993).
[8] H. Partridge, C. W. Bauschlicher, Jr., and J. R. Stallcop, J. Chem. Phys. **99**, 5951 (1993).
[9] A. I. Boothroyd, W. J. Keogh, P. G. Martin, and M. R. Peterson, J. Chem. Phys. **104**, 7139 (1996).
[10] J. Komasa, W. Cencek, and J. Rychlewski, Comput. Methods Sci. Technol. **2**, 87 (1996).
[11] Y.-S. M. Wu, A. Kuppermann, and J. B. Anderson, Phys. Chem. Chem. Phys. **1**, 929 (1999).
[12] J. S. Lee, Chem. Phys. Lett. **339**, 133 (2001).
[13] S. L. Mielke, B. C. Garrett, and K. A. Peterson, J. Chem. Phys. **116**, 4142 (2002).
[14] W. A. Al-Saidi, H. Krakauer, and S. W. Zhang, J. Chem. Phys. **126**, 194105 (2007).
[15] J. B. Anderson, J. Chem. Phys. **144**, 166101 (2016).
[16] G. Halasz, A. Vibok, A. M. Mebel, and M. Baer, J. Chem. Phys. **118**, 3052 (2003).
[17] T. Vertesi, A. Vibok, G. J. Halasz, and M. Baer, J. Chem. Phys. **120**, 8420 (2004).
[18] S. L. Mielke, D. W. Schwenke, G. C. Schatz, B. C. Garrett, and K. A. Peterson, J. Phys. Chem. A **113**, 4479 (2009).
[19] R. W. Patch, J. Chem. Phys. **59**, 6468 (1973).
[20] M. Gustafsson, L. Frommhold, and W. Meyer, J. Chem. Phys. **118**, 1667 (2003).
[21] H.-J. Werner, P. J. Knowles, G. Knizia, F. R. Manby, M. Schütz, P. Celani, W. Györffy, D. Kats, T. Korona, R. Lindh, A. Mitrushenkov, G. Rauhut, K. R. Shamasundar, T. B. Adler, R. D. Amos, S. Bennie, A. Bernhardsson, A. Berning, D. L. Cooper, M. J. O. Deegan, A. J. Dobbyn, F. Eckert, E. Goll, C. Hampel, A. Hesselmann, G. Hetzer, T. Hrenar, G. Jansen, C. Köppl, S. J. R. Lee, Y. Liu, A. W. Lloyd, Q. Ma, R. A. Mata, A. J. May, S. J. McNicholas, W. Meyer, T. F. Miller III, M. E. Mura, A. Nicklaß, D. P. O'Neill, P. Palmieri, D. Peng, K. Pflüger, R. Pitzer, M. Reiher, T. Shiozaki, H. Stoll, A. J. Stone, R. Tarroni, T. Thorsteinsson, M. Wang, and M. Welborn, MOLPRO, version 2015.1, a package of *ab initio* programs, 2015, see http://www.molpro.net.
[22] J. D. Poll and J. Van Kranendonk, Can. J. Phys. **39**, 189 (1961).
[23] J. E. Bohr and K. L. C. Hunt, J. Chem. Phys. **86**, 5441 (1987).
[24] T. Bancewicz, Chem. Phys. Lett. **244**, 305 (1995).
[25] T. Bancewicz, J. Chem. Phys. **134**, 104309 (2011).
[26] R. P. Feynman, Phys. Rev. **56**, 340 (1939).
[27] W. Byers Brown and D. M. Whisnant, Mol. Phys. **25**, 1385 (1973).
[28] K. L. C. Hunt, Chem. Phys. Lett. **70**, 336 (1980).
[29] L. Galatry and T. Gharbi, Chem. Phys. Lett. **75**, 427 (1980).
[30] D. P. Craig and T. Thirunamachandran, Chem. Phys. Lett. **80**, 14 (1981).
[31] K. L. C. Hunt and J. E. Bohr, J. Chem. Phys. **83**, 5198 (1985).
[32] K. L. C. Hunt, J. Chem. Phys. **92**, 1180 (1990).
[33] P. W. Fowler, Chem. Phys. **143**, 447 (1990).
[34] D. M. Bishop and J. Pipin, J. Chem. Phys. **98**, 4003 (1993).
[35] R. W. Patch, J. Quant. Spectrosc. Radiat. Transfer **14**, 49 (1974).
[36] M. Gustafsson and L. Frommhold, Astron. Astrophys. **400**, 1161 (2003).
[37] M. F. Crawford, H. L. Welsh, and J. L. Locke, Phys. Rev. **75**, 1607 (1949).
[38] H. L. Welsh, M. F. Crawford, and J. L. Locke, Phys. Rev. **76**, 580 (1949).
[39] H. L. Welsh, M. F. Crawford, J. C. F. MacDonald, and D. A. Chisholm, Phys. Rev. **83**, 1264 (1951).
[40] J. A. A. Ketelaar, J. P. Colpa, and F. N. Hooge, J. Chem. Phys. **23**, 413 (1955).
[41] A. R. W. McKellar, J. W. McTaggart, and H. L. Welsh, Can. J. Phys. **53**, 2060 (1975).
[42] G. Birnbaum, G. Bachet, and L. Frommhold, Phys. Rev. A **36**, 3729 (1987).
[43] C. Brodbeck, N. van-Thanh, J.-P. Bouanich, and L. Frommhold, Phys. Rev. A **51**, 1209 (1995).
[44] M. F. Crawford, H. L. Welsh, J. C. F. MacDonald, and J. L. Locke, Phys. Rev. **80**, 469 (1950).
[45] S. P. Reddy and K. S. Chang, J. Mol. Spectrosc. **47**, 22 (1973).
[46] G. Birnbaum, J. Quant. Spectrosc. Radiat. Transfer **19**, 51 (1978).
[47] J. P. Bouanich, C. Brodbeck, P. Drossart, and E. Lellouch, J. Quant. Spectrosc. Radiat. Transfer **42**, 141 (1989).
[48] J.-P. Bouanich, C. Brodbeck, N. van-Thanh, and P. Drossart, J. Quant. Spectrosc. Radiat. Transfer **44**, 393 (1990).
[49] S. P. Reddy and W. F. Lee, Can. J. Phys. **46**, 1373 (1968).
[50] U. Buontempo, P. Codastefano, S. Cunsolo, P. Dore, and P. Maselli, Can. J. Phys. **61**, 156 (1983).
[51] P. Dore, A. Filabozzi, and G. Birnbaum, Can. J. Phys. **66**, 803 (1988).
[52] P. Dore, A. Filabozzi, and G. Birnbaum, Can. J. Phys. **67**, 599 (1989).
[53] R. D. G. Prasad, P. G. Gillard, and S. P. Reddy, J. Chem. Phys. **107**, 4906 (1997).

[54]G. Varghese and S. P. Reddy, Can. J. Phys. **47**, 2745 (1969).
[55]H. P. Gush, W. F. J. Hare, E. J. Allin, and H. L. Welsh, Can. J. Phys. **38**, 176 (1960).
[56]D. H. Rank, T. A. Wiggins, P. Sitaram, A. F. Slomba, and B. S. Rao, J. Opt. Soc. Am. **52**, 1004 (1962).
[57]J. L. Hunt and H. L. Welsh, Can. J. Phys. **42**, 873 (1964).
[58]D. R. Bosomworth and H. P. Gush, Can. J. Phys. **43**, 751 (1965).
[59]A. Watanabe and H. L. Welsh, Can. J. Phys. **43**, 818 (1965).
[60]A. Watanabe and H. L. Welsh, Can. J. Phys. **45**, 2859 (1967).
[61]A. Watanabe, J. L. Hunt, and H. L. Welsh, Can. J. Phys. **49**, 860 (1971).
[62]A. Watanabe, Can. J. Phys. **49**, 1320 (1971).
[63]P. W. Gibbs, C. G. Gray, J. L. Hunt, S. P. Reddy, R. H. Tipping, and K. S. Chang, Phys. Rev. Lett. **33**, 256 (1974).
[64]S. P. Reddy, G. Varghese, and R. D. G. Prasad, Phys. Rev. A **15**, 975 (1977).
[65]A. Sen, R. D. G. Prasad, and S. P. Reddy, J. Chem. Phys. **72**, 1716 (1980).
[66]S. P. Reddy, A. Sen, and R. D. G. Prasad, J. Chem. Phys. **72**, 6102 (1980).
[67]P. M. Silvaggio, D. Goorvitch, and R. W. Boese, J. Quant. Spectrosc. Radiat. Transfer **26**, 103 (1981).
[68]G. Bachet, E. R. Cohen, P. Dore, and G. Birnbaum, Can. J. Phys. **61**, 591 (1983).
[69]P. Dore, L. Nencini, and G. Birnbaum, J. Quant. Spectrosc. Radiat. Transfer **30**, 245 (1983).
[70]A. R. W. McKellar, Can. J. Phys. **66**, 155 (1988).
[71]J. Schaefer and A. R. W. McKellar, Z. Phys. D: At., Mol. Clusters **15**, 51 (1990); **17**, 231 (1990).
[72]C. Brodbeck, N. van-Thanh, A. Jean-Louis, J.-P. Bouanich, and L. Frommhold, Phys. Rev. A **50**, 484 (1994).
[73]C. Brodbeck, J.-P. Bouanich, N. van-Thanh, Y. Fu, and A. Borysow, J. Chem. Phys. **110**, 4750 (1999).
[74]M. Gustafsson, L. Frommhold, D. Bailly, J.-P. Bouanich, and C. Brodbeck, J. Chem. Phys. **119**, 12264 (2003).
[75]R. Krech, G. Caledonia, S. Schertzer, K. Ritter, T. Wilkerson, L. Cotnoir, R. Taylor, and G. Birnbaum, Phys. Rev. Lett. **49**, 1913 (1982).
[76]G. E. Caledonia, R. H. Krech, T. D. Wilkerson, R. L. Taylor, and G. Birnbaum, Phys. Rev. A **43**, 6010 (1991).
[77]D. Hammer, L. Frommhold, and W. Meyer, J. Chem. Phys. **111**, 6283 (1999).
[78]D. Hammer and L. Frommhold, J. Chem. Phys. **112**, 654 (2000).
[79]L. Frommhold, M. Abel, F. Wang, M. Gustafsson, X. Li, and K. L. C. Hunt, Mol. Phys. **108**, 2265 (2010).
[80]G. C. Tabisz, in *Molecular Spectroscopy*, Specialist Periodical Reports, edited by R. F. Barrow, D. A. Long, and J. Sheridan (Chemical Society, London, 1979), Vol. 6, p. 136.
[81]Y. Le Duff and R. Ouillon, J. Chem. Phys. **82**, 1 (1985).
[82]M. S. Brown, M. H. Proffitt, and L. Frommhold, Chem. Phys. Lett. **117**, 243 (1985).
[83]M. S. Brown and L. Frommhold, Chem. Phys. Lett. **127**, 197 (1986).
[84]M. Moraldi, A. Borysow, and L. Frommhold, J. Chem. Phys. **88**, 5344 (1988).
[85]A. Borysow and M. Moraldi, Phys. Rev. A **40**, 1251 (1989).
[86]U. Bafile, M. Zoppi, F. Barocchi, M. S. Brown, and L. Frommhold, Phys. Rev. A **40**, 1654 (1989).
[87]M. S. Brown, S. K. Wang, and L. Frommhold, Phys. Rev. A **40**, 2276 (1989).
[88]M. S. Brown and L. Frommhold, Mol. Phys. **66**, 527 (1989).
[89]U. Bafile, L. Ulivi, M. Zoppi, F. Barocchi, M. Moraldi, and A. Borysow, Phys. Rev. A **42**, 6916 (1990).
[90]L. Frommhold, J. D. Poll, and R. H. Tipping, Phys. Rev. A **46**, 2955 (1992).
[91]A. Borysow and M. Moraldi, Phys. Rev. A **48**, 3036 (1993).
[92]M. Gustafsson, L. Frommhold, X. Li, and K. L. C. Hunt, J. Chem. Phys. **130**, 164314 (2009).
[93]P. Kaatz and D. P. Shelton, Mol. Phys. **88**, 683 (1996).
[94]A. R. W. McKellar, J. Chem. Phys. **93**, 18 (1990).
[95]A. R. W. McKellar, Chem. Phys. Lett. **186**, 58 (1991).
[96]M. Abu-Kharma, C. Stamp, G. Varghese, and S. P. Reddy, J. Quant. Spectrosc. Radiat. Transfer **97**, 332 (2006).
[97]P. Jankowski, A. R. W. McKellar, and K. Szalewicz, Science **336**, 1147 (2012).
[98]P. Jankowski, L. A. Surin, A. Potapov, S. Schlemmer, A. R. W. McKellar, and K. Szalewicz, J. Chem. Phys. **138**, 084307 (2013).
[99]A. R. W. McKellar, J. Chem. Phys. **136**, 094305 (2012).
[100]A. Borysow, L. Frommhold, and P. Dore, J. Chem. Phys. **85**, 4750 (1986).
[101]P. Codastefano, P. Dore, and L. Nencini, J. Quant. Spectrosc. Radiat. Transfer **36**, 239 (1986).
[102]H. Tran, P.-M. Flaud, T. Fouchet, T. Gabard, and J.-M. Hartmann, J. Quant. Spectrosc. Radiat. Transfer **101**, 306 (2006).
[103]G. Birnbaum, A. Borysow, and H. G. Sutter, J. Quant. Spectrosc. Radiat. Transfer **38**, 189 (1987).
[104]R. E. Samuelson, N. Nath, and A. Borysow, Planet. Space Sci. **45**, 959 (1997).
[105]P. Dore, A. Borysow, and L. Frommhold, J. Chem. Phys. **84**, 5211 (1986).
[106]P. Codastefano and P. Dore, J. Quant. Spectrosc. Radiat. Transfer **36**, 445 (1986).
[107]D. Bailly, G. Birnbaum, A. Buechele, P.-M. Flaud, and J.-M. Hartmann, J. Quant. Spectrosc. Radiat. Transfer **83**, 1 (2004).
[108]S. P. Reddy and C. W. Cho, Can. J. Phys. **43**, 793 (1965).
[109]S. T. Pai, S. P. Reddy, and C. W. Cho, Can. J. Phys. **44**, 2893 (1966).
[110]S. P. Reddy and C. Z. Kuo, J. Mol. Spectrosc. **37**, 327 (1971).
[111]W. E. Russell, S. P. Reddy, and C. W. Cho, J. Mol. Spectrosc. **52**, 72 (1974).
[112]A. R. W. McKellar, J. Chem. Phys. **61**, 4636 (1974).
[113]R. D. G. Prasad and S. P. Reddy, J. Chem. Phys. **62**, 3582 (1975).
[114]J. D. Poll, R. H. Tipping, R. D. G. Prasad, and S. P. Reddy, Phys. Rev. Lett. **36**, 248 (1976).
[115]R. D. G. Prasad and S. P. Reddy, J. Chem. Phys. **65**, 83 (1976).
[116]R. D. G. Prasad and S. P. Reddy, J. Chem. Phys. **66**, 707 (1977).
[117]S. P. Reddy and R. D. G. Prasad, J. Chem. Phys. **66**, 5259 (1977).
[118]U. Buontempo, P. Codastefano, S. Cunsolo, P. Dore, and P. Maselli, Can. J. Phys. **59**, 1495 (1981).
[119]R. J. Penney, R. D. G. Prasad, and S. P. Reddy, J. Chem. Phys. **77**, 131 (1982).
[120]P. G. Gillard, R. D. G. Prasad, and S. P. Reddy, J. Chem. Phys. **81**, 3458 (1984).
[121]G. Varghese, C. Stamp, and S. P. Reddy, J. Quant. Spectrosc. Radiat. Transfer **87**, 387 (2004).
[122]M. Abu-Kharma, G. Varghese, and S. P. Reddy, J. Mol. Spectrosc. **232**, 369 (2005).
[123]M. Abu-Kharma and S. P. Reddy, J. Mol. Spectrosc. **233**, 133 (2005).
[124]M. Abu-Kharma, C. Stamp, S. P. Reddy, N. Sahwagfeh, and H. Y. Omari, J. Phys. B: At., Mol. Opt. Phys. **43**, 135104 (2010).
[125]M. Abu-Kharma, H. Y. Omari, N. Shawaqfeh, and C. Stamp, J. Mol. Spectrosc. **259**, 111 (2010).
[126]A. Watanabe and H. L. Welsh, Phys. Rev. Lett. **13**, 810 (1964).
[127]A. R. W. McKellar and H. L. Welsh, Proc. R. Soc. A **322**, 421 (1971).
[128]A. R. W. McKellar and H. L. Welsh, Can. J. Phys. **52**, 1082 (1974).
[129]A. R. W. McKellar, J. Chem. Phys. **92**, 3261 (1990).
[130]A. R. W. McKellar and J. Schaefer, J. Chem. Phys. **95**, 3081 (1991).
[131]A. Kudian, H. L. Welsh, and A. Watanabe, J. Chem. Phys. **43**, 3397 (1965).
[132]A. K. Kudian and H. L. Welsh, Can. J. Phys. **49**, 230 (1971).
[133]A. R. W. McKellar and H. L. Welsh, Can. J. Phys. **50**, 1458 (1972).
[134]A. R. W. McKellar, Icarus **80**, 361 (1989).
[135]A. R. W. McKellar, J. Chem. Phys. **105**, 2628 (1996).
[136]A. R. W. McKellar, J. Chem. Phys. **122**, 084320 (2005).
[137]A. R. W. McKellar, Can. J. Phys. **87**, 411 (2009).
[138]A. R. W. McKellar, Can. J. Phys. **91**, 957 (2013).
[139]A. Potapov, A. Sánchez-Monge, P. Schilke, U. U. Graf, T. Möller, and S. Schlemmer, Astron. Astrophys. **594**, A117 (2016).
[140]S. P. Reddy, F. Xiang, and G. Varghese, Phys. Rev. Lett. **74**, 367 (1995).
[141]M. Moraldi and L. Frommhold, Phys. Rev. A **40**, 6260 (1989).
[142]M. Moraldi and L. Frommhold, Phys. Rev. Lett. **74**, 363 (1995).
[143]M. Moraldi and L. Frommhold, J. Chem. Phys. **103**, 2377 (1995).
[144]X. Li and K. L. C. Hunt, J. Chem. Phys. **107**, 4133 (1997).

[145]J. Van Kranendonk, *Solid Hydrogen* (Plenum, New York, 1983).
[146]G. Varghese, R. D. G. Prasad, and S. P. Reddy, Phys. Rev. A **35**, 701 (1987).
[147]M. C. Chan, M. Okumura, C. M. Gabrys, L. W. Xu, B. D. Rehfuss, and T. Oka, Phys. Rev. Lett. **66**, 2060 (1991).
[148]M. C. Chan, S. S. Lee, M. Okumura, and T. Oka, J. Chem. Phys. **95**, 88 (1991).
[149]T. Oka, Annu. Rev. Phys. Chem. **44**, 299 (1993).
[150]D. P. Weliky, T. J. Byers, K. E. Kerr, T. Momose, R. M. Dickson, and T. Oka, Appl. Phys. B: Lasers Opt. **59**, 265 (1994).
[151]R. M. Dickson and T. Oka, J. Phys. Chem. **99**, 2617 (1995).
[152]D. P. Weliky, K. E. Kerr, T. J. Byers, Y. Zhang, T. Momose, and T. Oka, J. Chem. Phys. **105**, 4461 (1996).
[153]R. D. G. Prasad, M. J. Clouter, and S. P. Reddy, Phys. Rev. A **17**, 1690 (1978).
[154]M. Okamura, M. C. Chan, and T. Oka, Phys. Rev. Lett. **62**, 32 (1989).
[155]N. H. Rich and A. R. W. McKellar, Can. J. Phys. **54**, 486 (1976).
[156]J. L. Hunt and J. D. Poll, Mol. Phys. **59**, 163 (1986).
[157]A. Borysow and L. Frommhold, Adv. Chem. Phys. **75**, 439 (1989).
[158]W. Meyer and L. Frommhold, Phys. Rev. A **34**, 2771 (1986).
[159]W. Meyer and L. Frommhold, Phys. Rev. A **34**, 2936 (1986).
[160]L. Frommhold and W. Meyer, Phys. Rev. A **35**, 632 (1987).
[161]A. Borysow, L. Frommhold, and W. Meyer, J. Chem. Phys. **88**, 4855 (1988).
[162]W. Meyer, L. Frommhold, and G. Birnbaum, Phys. Rev. A **39**, 2434 (1989).
[163]W. Meyer, A. Borysow, and L. Frommhold, Phys. Rev. A **40**, 6931 (1989).
[164]A. Borysow, L. Frommhold, and W. Meyer, Phys. Rev. A **41**, 264 (1990).
[165]Y. Fu, C. Zheng, and A. Borysow, J. Quant. Spectrosc. Radiat. Transfer **67**, 303 (2000), with *ab initio* results listed at www.astro.ku.dk/~aborysow/data/index.html.
[166]T. Bancewicz and G. Maroulis, Phys. Rev. A **79**, 042704 (2009).
[167]A. Haskopoulos and G. Maroulis, Chem. Phys. **367**, 127 (2010).
[168]X. Li, J. F. Harrison, M. Gustafsson, F. Wang, M. Abel, L. Frommhold, and K. L. C. Hunt, AIP Conf. Proc. **1504**, 100 (2012).
[169]X. Li, A. Mandal, E. Miliordos, and K. L. C. Hunt, J. Chem. Phys. **136**, 044320 (2012).
[170]A. Haskopoulos, G. Maroulis, and T. Bancewicz, J. Mol. Model. **24**, 265 (2018).
[171]G. Maroulis, J. Phys. Chem. A **104**, 4772 (2000).
[172]X. Li, C. Ahuja, J. F. Harrison, and K. L. C. Hunt, J. Chem. Phys. **126**, 214302 (2007).
[173]T. Bancewicz and G. Maroulis, Chem. Phys. Lett. **471**, 148 (2009).
[174]W. Głaz, T. Bancewicz, J.-L. Godet, M. Gustafsson, A. Haskopoulos, and G. Maroulis, J. Chem. Phys. **145**, 034303 (2016).
[175]G. Maroulis and A. Haskopoulos, Chem. Phys. Lett. **349**, 335 (2001).
[176]J.-L. Godet, T. Bancewicz, W. Głaz, G. Maroulis, and A. Haskopoulos, J. Chem. Phys. **131**, 204305 (2009).
[177]T. Bancewicz and G. Maroulis, Chem. Phys. Lett. **498**, 349 (2010).
[178]W. Meyer, A. Borysow, and L. Frommhold, Phys. Rev. A **47**, 4065 (1993).
[179]M. Gustafsson, L. Frommhold, and W. Meyer, J. Chem. Phys. **113**, 3641 (2000).
[180]M. Abel, L. Frommhold, X. Li, and K. L. C. Hunt, J. Phys. Chem. A **115**, 6805 (2011).
[181]M. Abel, L. Frommhold, X. P. Li, and K. L. C. Hunt, J. Chem. Phys. **136**, 044319 (2012).
[182]T. Karman, A. van der Avoird, and G. C. Groenenboom, J. Chem. Phys. **142**, 084305 (2015).
[183]W. Meyer and L. Frommhold, J. Chem. Phys. **143**, 114313 (2015).
[184]T. Karman, E. Miliordos, K. L. C. Hunt, G. C. Groenenboom, and A. van der Avoird, J. Chem. Phys. **142**, 084306 (2015).
[185]T. Karman, A. van der Avoird, and G. C. Groenenboom, J. Chem. Phys. **147**, 084306 (2017).
[186]T. Karman, M. A. J. Koenis, A. Banerjee, D. H. Parker, I. E. Gordon, A. van der Avoird, W. J. van der Zande, and G. C. Groenenboom, Nat. Chem. **10**, 549 (2018); **10**, 573 (2018).
[187]M. S. A. El-Kader, G. Maroulis, and E. Bich, Chem. Phys. **403**, 37 (2012).
[188]M. S. A. El-Kader and G. Maroulis, Chem. Phys. Lett. **684**, 141 (2017).
[189]M. S. A. El-Kader, J.-L. Godet, A. A. El-Sadek, and G. Maroulis, Mol. Phys. **115**, 2614 (2017).
[190]M. S. A. El-Kader, J.-L. Godet, M. Gustafsson, and G. Maroulis, J. Quant. Spectrosc. Radiat. Transfer **209**, 232 (2018).
[191]S. L. Mielke, K. A. Peterson, D. W. Schwenke, B. C. Garrett, D. G. Truhlar, J. V. Michael, M. C. Su, and J. W. Sutherland, Phys. Rev. Lett. **91**, 063201 (2003).
[192]S. A. Wrathmall, A. Gusdorf, and D. R. Flower, Mon. Not. R. Astron. Soc. **382**, 133 (2007).
[193]L. M. Trafton, Astrophys. J. **140**, 1340 (1964).
[194]B. M. S. Hansen, Nature **394**, 860 (1998).
[195]D. Saumon and S. B. Jacobson, Astrophys. J. **511**, L107 (1999).
[196]S. T. Hodgkin, B. R. Oppenheimer, N. C. Hambly, R. F. Jameson, S. J. Smartt, and I. A. Steele, Nature **403**, 57 (2000).
[197]G. P. Kuiper, Astrophys. J. **109**, 540 (1949).
[198]G. Herzberg, Astrophys. J. **115**, 337 (1952).
[199]A. R. W. McKellar, Astrophys. J. **326**, L75 (1988).
[200]P. Bergeron, M.-T. Ruiz, S. K. Leggett, D. Saumon, and F. Wesemael, Astrophys. J. **423**, 456 (1994).
[201]P. Bergeron, D. Saumon, and F. Wesemael, Astrophys. J. **443**, 764 (1995).
[202]H. C. Harris, C. C. Dahn, F. J. Vrba, A. A. Henden, J. Liebert, G. D. Schmidt, and I. N. Reid, Astrophys. J. **524**, 1000 (1999).
[203]P. Bergeron and S. K. Leggett, Astrophys. J. **580**, 1070 (2002).
[204]J. Farihi, Astrophys. J. **610**, 1013 (2004).
[205]D. Saumon, M. S. Marley, M. Abel, L. Frommhold, and R. S. Freedman, Astrophys. J. **750**, 74 (2012).
[206]I. E. Gordon, L. S. Rothman, C. Hill, R. V. Kochanov, Y. Tan, P. F. Bernath, M. Birk, V. Boudon, A. Campargue, K. V. Chance, B. J. Drouin, J.-M. Flaud, R. R. Gamache, J. T. Hodges, D. Jacquemart, V. I. Perevalov, A. Perrin, K. P. Shine, M. A. H. Smith, J. Tennyson, G. C. Toon, H. Tran, V. G. Tyuterev, A. Barbe, A. G. Császár, V. M. Devi, T. Furtenbacher, J. J. Harrison, J.-M. Hartmann, A. Jolly, T. J. Johnson, T. Karman, I. Kleiner, A. A. Kyuberis, J. Loos, O. M. Lyulin, S. T. Massie, S. N. Mikhailenko, N. Moazzen-Ahmadi, H. S. P. Müller, O. V. Naumenko, A. V. Nikitin, O. L. Polyansky, M. Rey, M. Rotger, S. W. Sharpe, K. Sung, E. Starikova, S. A. Tashkun, J. Vander Auwera, G. Wagner, J. Wilzewski, P. Wcisło, S. Yu, and E. J. Zak, J. Quant. Spectrosc. Radiat. Transfer **203**, 3 (2017).
[207]W. Kowalski and D. Saumon, Astrophys. J. **651**, L137 (2006).
[208]R. D. Rohrmann, L. G. Althaus, and S. O. Kepler, Mon. Not. R. Astron. Soc. **411**, 781 (2011).
[209]J. L. Linsky, Astrophys. J. **156**, 989 (1969).
[210]C.-Y. Hu, T. Naab, S. Walch, S. C. O. Glover, and P. C. Clark, Mon. Not. R. Astron. Soc. **458**, 3528 (2016).
[211]S. Bialy, B. Burkhart, and A. Sternberg, Astrophys. J. **843**, 92 (2017).
[212]B. Diemer, A. R. H. Stevens, J. C. Forbes, F. Marinacci, L. Hernquist, C. D. Lagos, A. Sternberg, A. Pillepich, D. Nelson, G. Popping, F. Villaescusa-Navarro, P. Torrey, and M. Vogelsberger, Astrophys. J., Suppl. Ser. **238**, 33 (2018).
[213]L. Z. Xie, G. De Lucia, M. Hirschmann, F. Fontanot, and A. Zoldan, Mon. Not. R. Astron. Soc. **469**, 968 (2017).
[214]L. Cortese, B. Catinella, and S. Janowiecki, Astrophys. J. **848**, L7 (2017).
[215]B. Catinella, A. Saintonge, S. Janowiecki, L. Cortese, R. Dave, J. J. Lemonias, A. P. Cooper, D. Schiminovich, C. B. Hummels, S. Fabello, K. Gereb, V. Kilborn, and J. Wang, Mon. Not. R. Astron. Soc. **476**, 875 (2018).
[216]B. Catinella and L. Cortese, Mon. Not. R. Astron. Soc. **446**, 3526 (2015).
[217]S. L. Ellison, B. Catinella, and L. Cortese, Mon. Not. R. Astron. Soc. **478**, 3447 (2018).
[218]A. R. H. Stevens, C. D. Lagos, D. Obreschkow, and M. Sinha, Mon. Not. R. Astron. Soc. **481**, 5543 (2018).
[219]A. L. Broadfoot, M. J. S. Belton, P. Z. Takacs, B. R. Sandel, D. E. Shemansky, J. B. Holberg, J. M. Ajello, S. K. Atreya, T. M. Donahue, H. W. Moos, J. L. Bertaux, J. E. Blamont, D. F. Strobel, J. C. McConnell, A. Dalgarno, R. Goody, and M. B. McElroy, Science **204**, 979 (1979).
[220]A. L. Broadfoot, B. R. Sandel, D. E. Shemansky, J. B. Holberg, G. R. Smith, D. F. Strobel, J. C. McConnell, S. Kumar, D. M. Hunten, S. K. Atreya, T. M. Donahue,

H. W. Moos, J. L. Bertaux, J. E. Blamont, R. B. Pomphrey, and S. Linick, Science **212**, 206 (1981).
[221]C. A. Barth, C. W. Hord, A. I. F. Stewart, W. R. Pryor, K. E. Simmons, W. E. McClintock, J. M. Aiello, K. L. Naviaux, and J. J. Aiello, Geophys. Res. Lett. **24**, 2147, https://doi.org/10.1029/97gl01927 (1997).
[222]J. Alday, L. Roth, N. Ivchenko, K. D. Retherford, T. M. Becker, P. Molyneux, and J. Saur, Planet. Space Sci. **148**, 35 (2017).
[223]L. Roth, J. Alday, T. M. Becker, N. Ivchenko, and K. D. Retherford, J. Geophys. Res.: Planets **122**, 1046, https://doi.org/10.1002/2017je005294 (2017).
[224]L. Roth, K. D. Retherford, N. Ivchenko, N. Schlatter, D. F. Strobel, T. M. Becker, and C. Grava, Astron. J. **153**, 67 (2017).
[225]D. F. Strobel and B. C. Wolven, Astrophys. Space Sci. **277**, 271 (2001).
[226]W. L. Tseng, R. E. Johnson, and W. H. Ip, Planet. Space Sci. **85**, 164 (2013).
[227]J. Q. Qin and L. Waldrop, Nat. Commun. **7**, 13655 (2016).
[228]M.-C. Liang, C. D. Parkinson, A. Y.-T. Lee, Y. L. Yung, and S. Seager, Astrophys. J. **596**, L247 (2003).
[229]D. Ehrenriech, A. L. des Etangs, G. Hebrard, J.-M. Desert, A. Vidal-Madjar, J. C. McConnell, C. D. Parkinson, G. E. Ballester, and R. Ferlet, Astron. Astrophys. **483**, 933 (2008).
[230]L. Ben-Jaffel, Astrophys. J. **688**, 1352 (2008).
[231]A. L. des Etangs, D. Ehrenreich, A. Vidal-Madjar, G. E. Ballester, J.-M. Desert, R. Ferlet, G. Hebrard, D. K. Sing, K.-O. Tchakoumegni, and S. Udry, Astron. Astrophys. **514**, A72 (2010).
[232]T. T. Koskinen, A. D. Aylward, and S. Miller, Astrophys. J. **693**, 868 (2009).
[233]C. L. Huang, P. Arras, D. Christie, and Z. Y. Li, Astrophys. J. **851**, 150 (2017).
[234]R. A. Murray-Clay, E. I. Chiang, and N. Murray, Astrophys. J. **693**, 23 (2009).
[235]H. Lammer, P. Odert, M. Leitzinger, M. L. Khodachenko, M. Panchenko, Y. L. Kulikov, T. L. Zhang, H. I. M. Lichtenegger, N. V. Erkaev, G. Wuchterl, G. Micela, T. Penz, H. K. Biernat, J. Weingrill, M. Steller, H. Ottacher, J. Hasiba, and A. Hanslmeier, Astron. Astrophys. **506**, 399 (2009).
[236]D. Ehrenreich, V. Bourrier, P. J. Wheatley, A. L. des Etangs, G. Hebrard, S. Udry, X. Bonfils, X. Delfosse, J. M. Desert, D. K. Sing, and A. Vidal-Madjar, Nature **522**, 459 (2015).
[237]D. Dragomir, B. Benneke, K. A. Pearson, I. J. M. Crossfield, J. Eastman, T. Barman, and L. I. Biddle, Astrophys. J. **814**, 102 (2015).
[238]T. H. Dunning, Jr., J. Chem. Phys. **90**, 1007 (1989).
[239]K. A. Peterson, D. E. Woon, and T. H. Dunning, Jr., J. Chem. Phys. **100**, 7410 (1994).
[240]P. J. Knowles, C. Hampel, and H.-J. Werner, J. Chem. Phys. **99**, 5219 (1993); **112**, 3106 (2000).
[241]K. Raghavachari, G. W. Trucks, J. A. Pople, and M. Head-Gordon, Chem. Phys. Lett. **157**, 479 (1989).
[242]J. D. Watts, J. Gauss, and R. D. Bartlett, J. Chem. Phys. **98**, 8718 (1993).
[243]M. J. O. Deegan and P. J. Knowles, Chem. Phys. Lett. **227**, 321 (1994).
[244]P. J. Knowles and N. C. Handy, J. Phys. Chem. **92**, 3097 (1988).
[245]M. Rittby and R. J. Bartlett, J. Phys. Chem. **92**, 3033 (1988).
[246]G. E. Scuseria, Chem. Phys. Lett. **176**, 27 (1991).
[247]H. B. Schlegel, J. Phys. Chem. **92**, 3075 (1988).
[248]Molpro User's Manual, 6.11 Global Thresholds (GTHRESH).
[249]The collision-induced dipole is calculated as $\Delta\mu = 3/(2f)\ \{E(-f) - E(f) - 2^{-1/2}[E(-2^{1/2}\,f) - E(2^{1/2}\,f)] + 3^{-3/2}\ [E(-3^{1/2}\,f) - E(3^{1/2}\,f)]\}$.
[250]S. Huzinaga, J. Chem. Phys. **42**, 1293 (1964).
[251]W. Meyer, in *Phenomena Induced by Intermolecular Interactions*, edited by G. Birnbaum (Plenum, New York, 1985), p. 29.
[252]P. Güttinger, Z. Phys. **73**, 169 (1932).
[253]W. Pauli, Handbuch der Physik **24**, 162 (1933).
[254]H. Hellmann, *Einführung in die Quantenchemie* (Franz Deuticke, Leipzig, 1937), p. 285.
[255]T. U. Helgaker and J. Almlöf, Int. J. Quantum Chem. **26**, 275 (1984).
[256]D. Tzeli and A. Mavridis, J. Chem. Phys. **118**, 4984 (2003).
[257]E. Miliordos and K. L. C. Hunt, J. Chem. Phys. **149**, 234103 (2018).
[258]S. F. Boys and F. Bernardi, Mol. Phys. **19**, 553 (1970).
[259]W. Kolos and L. Wolniewicz, J. Chem. Phys. **46**, 1426 (1967).
[260]R. M. Berns and P. E. S. Wormer, Mol. Phys. **44**, 1215 (1981).
[261]J. Rychlewski, Mol. Phys. **41**, 833 (1980).
[262]A. Raj, H. Hamaguchi, and H. A. Witek, J. Chem. Phys. **148**, 104308 (2018).
[263]G. Karl, J. D. Poll, and L. Wolniewicz, Can. J. Phys. **53**, 1781 (1975).
[264]J. Komasa and A. J. Thakkar, Mol. Phys. **78**, 1039 (1993).
[265]S. A. Alexander and R. L. Coldwell, Int. J. Quantum Chem. **107**, 345 (2007).